DESIGN OF AMORPHOUS SOLID DISPERSIONS FOR THE SYNCHRONIZED RELEASE OF TWO DRUGS

A THESIS

SUBMITTED TO THE FACULTY OF THE GRADUATE SCHOOL

OF THE UNIVERSITY OF MINNESOTA

BY

JINGHAN LI

IN PARTIAL FULFILLMENT OF THE REQUIREMENTS

FOR THE DEGREE OF

MASTER OF SCIENCE

PROFESSOR. RAJ SURYANARAYANAN

DEC 2021

ACKNOWLEDGEMENT

Foremost, I would like to thank my advisor Dr. Raj Suryanarayanan for his patient guidance during my graduate study. His encouragement and valuable suggestions help me complete this project and overcome different research problems. I have deepened my understanding of solid-state pharmaceuticals by working with him.

Besides, I would like to thank my dissertation committee, Drs. Ronald Siegel and Chun Wang, for their inputs and valuable suggestions to my thesis.

I am also very grateful to Drs. Naga Kiran Duggirala and N. S. Krishna Kumar for their suggestions when developing this research project and valuable comments on my thesis. In addition, I appreciate all the generous help from Dr. Yongchao Su from Merck for the solid-state NMR experiments and data interpretation. I would also like to thank Drs. Dabing Chen and Li Zhong from Boehringer Ingelheim for their help with dissolution and HPLC studies.

I would also like to thank other Sury lab members, Dr. Bhushan Munjal, Dr. Navpreet Kaur, Jayesh Sonje, Rahul Lalge, who are like my siblings, for providing me with all kind suggestions and assistance. Besides, thank you, Katie, Jody, and Amanda for all the support from the department.

Finally, I would like to thank my family for their support and encouragement. I am very grateful to my important friends Shuming Zhang, Hanxun Wang, Peilun Zhang, Qishang Yu, and Yulu Tang, Yihan Wang, Lushan Wang and Liang Zhu, Ling Zhu, Ruoci Hu and Simseok A. Yuk, Ryoma Tanaka, Chenguang Wang, Xueyao Hu, Yafan Su, for their care

for my family and me. Finally, I would like to thank my girlfriend Dongyue Yu. You bring extra sunshine to my life and make me a good chef.

DEDICATION

For my loving grandparents and parents, Xian Li and Yueying Guo, Manwei Li and Xiangrong Zhang.

"Run to rescue with love and peace will follow."

--- *River Phoenix*

ABSTRACT

Purpose: To develop an amorphous solid dispersion (ASD) design strategy for poorly water soluble drug combinations.

Methods: Using sulfamethoxazole (SMZ) and trimethoprim (TMP) as the model drugs, a mixture of SMZ and TMP at weight ratios of 5:1 and 1:5 were formulated into ternary ASDs with an aminoalkyl methacrylate copolymer, Eudragit® E (EDE), and polyacrylic acid (PAA), respectively. The ASDs were characterized by thermal (differential scanning calorimetry, DSC), spectroscopic (dielectric and infrared spectroscopies, DES and IR) and X-ray diffractometric (XRD) techniques. The dissolution performance was evaluated under non-sink conditions using USP dissolution apparatus II method.

Results: Ternary ASDs were successfully prepared by solvent evaporation. Analyses of the glass transition temperature data of the binary (drug-drug) and ternary (drug-drug-polymer) systems implied strong drug-drug and drug-polymer interactions. The interactions resulted in a reduction in molecular mobility, evident from the increase in the structural (α-) relaxation time. The ionic SMZ-EDE and TMP-PAA interactions were characterized using IR. The ternary ASDs exhibited substantial enhancement in drug dissolution when compared with the crystalline mixtures. The ternary ASDs exhibited synchronized release.

Conclusion: The drug-drug and drug-polymer interactions improved the physical stability of the ternary ASDs by reducing molecular mobility. The proposed ASD design strategy could be a potential approach for the solubility enhancement of drug combinations with poor aqueous solubility.

Keywords

amorphous solid dispersion, coamorphous system, fixed-dose combination, dielectric spectroscopy, infrared spectroscopy, ionic interaction, hydrogen bonding, molecular mobility, dissolution, synchronized release

TABLE OF CONTENTS

LIST OF TABLES

LIST OF FIGURES

LIST OF ABBREVIATIONS

FDC: fixed-dose combination

API: active pharmaceutical ingredient

ASD: amorphous solid dispersion

SMZ: sulfamethoxazole

TMP: trimethoprim

EDE: Eudragit® EPO

PAA: polyacrylic acid

IR: infrared spectroscopy

DSC: differential scanning calorimetry

XRD: X-ray diffractometry

T_g: glass transition temperature

T_c: crystallization onset temperature

DES: dielectric spectroscopy

CHAPTER 1

INTRODUCTION

Amorphous pharmaceuticals

Up to 90% of the new chemical entities (NCEs), i.e. drugs under development, are poorly water soluble and belong to class II or IV of the Biopharmaceutics Classification System (BCS) [1]. Their poor solubility undermines the oral bioavailability as the drugs may not be in solution at the absorption site. Therefore, it becomes necessary to consider solubility enhancement strategies for drugs with solubility or dissolution rate limited oral bioavailability.

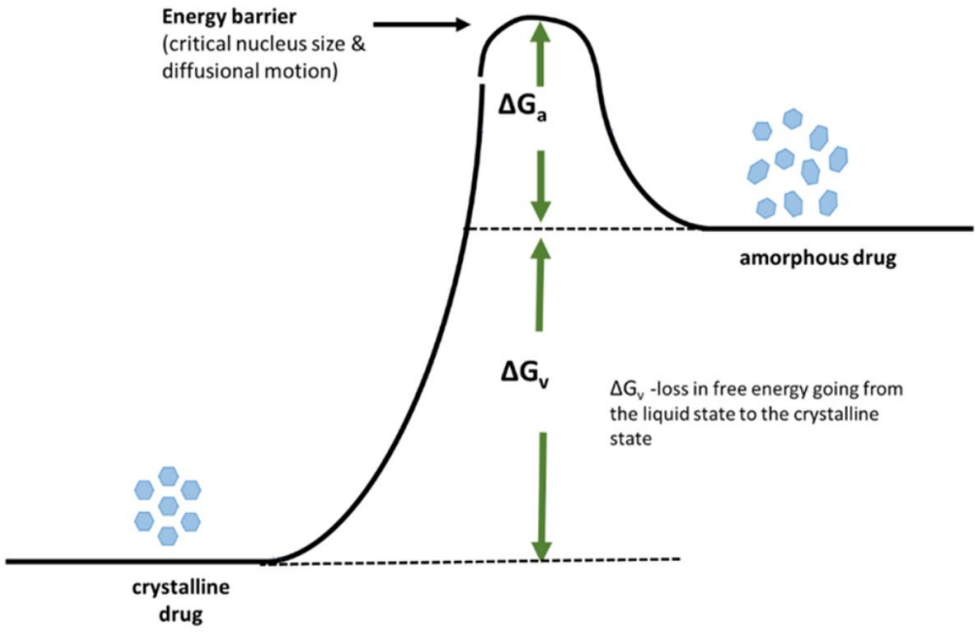

Figure 1. Schematic representation of energetics associated with nucleation and crystal growth from the amorphous state.

Figure reference: Newman A, et al, Molecular Pharmaceutics, 2020 [2].

Active pharmaceutical ingredients (APIs) in the crystalline state are stable, but the lattice energy acts as the main barrier for drug dissolution. On the other hand, molecules in the amorphous state lack long-range order and have high solubility. However, amorphous drug has the propensity to recrystallize due to its high free energy. The recrystallization process includes two continuous steps: nucleation and crystal growth. According to Figure 1, the activation energy, ΔG_a, acts as the energy barrier for nucleation. The loss in free energy going from the amorphous state to the crystalline state, ΔG_v, provides the main thermodynamic driving force for recrystallization [2].

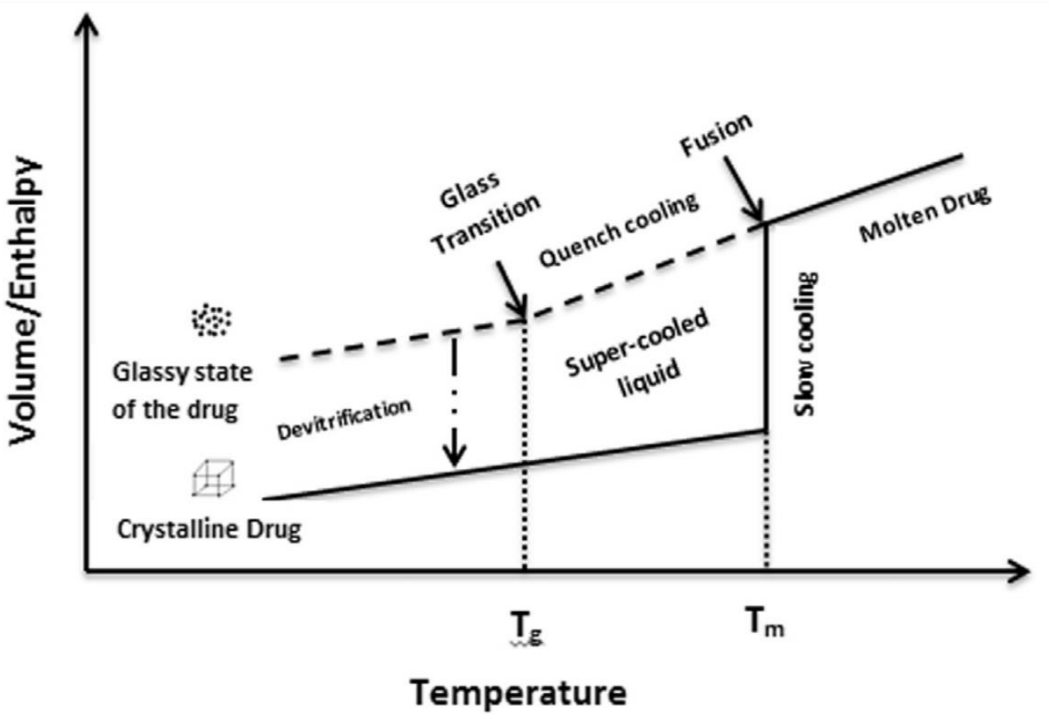

Figure 2. Enthalpy and volume of different states of drugs as a function of temperature; T_g and T_m are glass transition and melting temperature, respectively

Figure reference: Baghel S, et al, Journal of Pharmaceutical Sciences, 2016 [3].

When a crystalline drug is melted and then cooled, slow cooling may often provide enough time for the molecules to rearrange themselves back to their thermodynamically stable (crystalline) state. However, when the melt is rapidly cooled, it does not crystallize but forms a supercooled liquid below T_m. However, the system continues to be in "equilibrium" until reaching the glass transition temperature (T_g). On further cooling, the system falls out of equilibrium. The temperature dependence of volume and enthalpy in the supercooled and glassy states are very different (Figure 2) [3-4]. However, few drugs can be manufactured directly in the amorphous state. The high free energy can drive their recrystallization during downstream processing, transportation and storage.

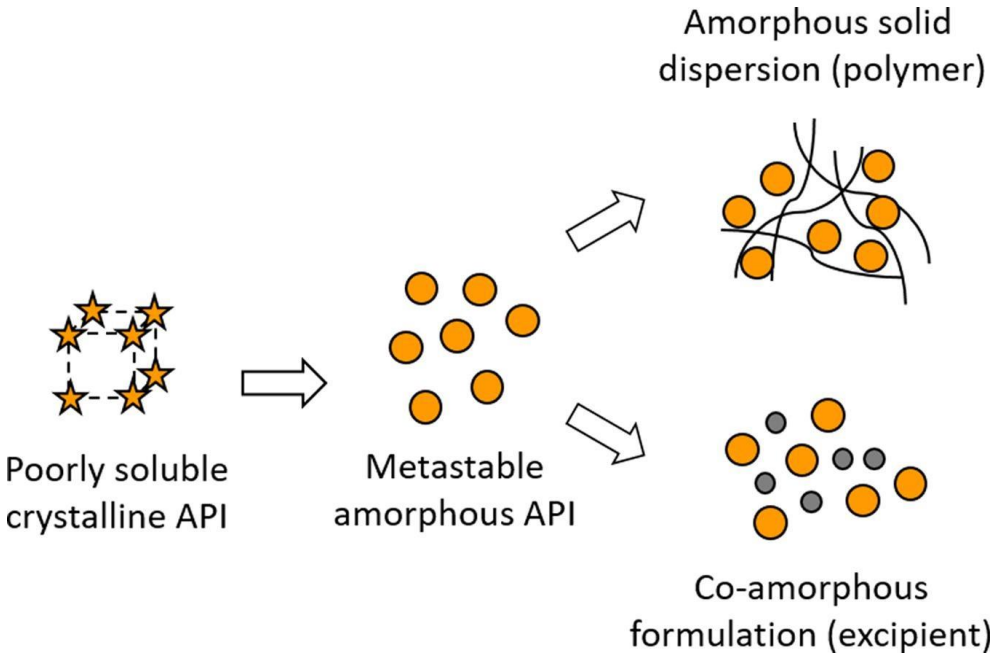

Figure 3. Schematic of crystalline and amorphous APIs, amorphous solid dispersion, and coamorphous formulation.

Figure reference: Han J, et al, Expert Opinion on Drug Delivery, 2020 [5].

In order to prevent recrystallization, drugs are often dispersed in polymers with a high T_g. When the drug is molecularly dispersed in the polymer, it is referred to as an amorphous solid dispersion (ASD) (Figure 3) [3]. The polymer, by interacting with the drug, kinetically "immobilizes" it in the matrix. The drug-polymer intermolecular interactions can cause a pronounced enhancement in viscosity of the system [3]. The weakly basic drug ketoconazole exhibited strong ionic interactions with polyacrylic acid (PAA) but weaker hydrogen bonding and dipole-dipole interactions with polyhydroxyethylmethacrylate (PHEMA), and polyvinylpyrrolidone (PVP). As a result, the enhancement of physical stability due to intermolecular interactions followed the rank order of PAA > PHEMA > PVP [6]. Currently, there are over 30 ASD products approved by the U.S. Food and Drug Administration (FDA)[7]. In addition to polymers, small molecule excipients, like organic acids and amino acids, can stabilize amorphous drugs by forming coamorphous systems (Figure 3) [5, 8]. These interactions, such as ionic interaction and hydrogen bonding, play an essential role in stabilizing the coamorphous systems.

The stabilization effect of intermolecular interaction can also be understood in the context of molecular mobility. The stronger the drug-polymer interaction, the more pronounced is the reduction in molecular mobility and the lower is the recrystallization tendency. The two relevant measures of molecular mobility – α-relaxation time (global molecular motions) and β-relaxation time (local molecular motions) can predict crystallization onset time in the supercool and glassy states, respectively [9-10]. Kothari et al. studied the correlation between the molecular mobility and physical stability of nifedipine ASDs. They tested three polymers: PVP, hydroxypropylmethyl cellulose (HPMCAS) and PAA. Among the polymers tested, nifedipine-PVP ASD with the strongest drug-polymer hydrogen bonding

showed the most pronounced increase in α-relaxation time and lowest crystallization propensity [11]. In addition to stabilizing the ASDs, the interactions, by inhibiting drug recrystallization in the dissolution medium, can sustain supersaturation [12]. Thus, the drug-polymer interaction can serve as a useful indicator for polymer selection. Such an approach has been successfully used in the design of ASDs. However, the situation gets complicated when a formulation contains more than one drug. For example, a fixed-dose combination (FDC) product includes two or more APIs in a single dosage form [13].

Drug combinations and their solubility enhancement

A drug combination may be warranted therapeutically, as is the case with sulfamethoxazole (SMZ) and trimethoprim (TMP). For patients on multiple drugs, FDC improves patient compliance by reducing the "pill burden" [13]. The problem with poor aqueous solubility can be exacerbated in drug combinations if both the APIs are poorly water-soluble. When considering solubility improvement strategies, the potential for drug-drug intermolecular interactions to enhance the solubility of both APIs can be explored. For some drug combinations, the APIs can form a drug-drug salt or cocrystal with each other. For example, artesunate formed a salt with either quinine or cinchonidine as a combination therapy to treat malaria [14]. Sulfonamides, a group of antibiotic drugs, can form either salts or cocrystals with TMP [15]. However, in salts and cocrystals, there is a defined molar ratio of the two components. For example, in a large fraction of cocrystals, there is a 1:1 molar ratio of drug to coformer. Thus, this approach will be practically feasible only if the dose of the two drugs in the combination is also in a 1:1 molar ratio, which is expected to be very rare. Unlike salts and cocrystals, amorphous mixtures do not need to follow a specific

molar stoichiometry. Drug-drug intermolecular interactions have formed the basis for an increasing number of coamorphous systems. Although flexible in composition, these systems tend to be most stable at some predefined stoichiometry. Deviation from this composition can cause a dramatic reduction in physical stability [16]. The addition of a polymer and formulating an ASD is a popular stabilization strategy and has yielded several marketed products such as Mavyret® (glecaprevir 100 mg + pibrentasvir 40 mg) and Harvoni® (ledipasvir 90 mg + sofosbuvir 400 mg) tablets [7].

STRATEGIES AND HYPOTHESIS

Although several FDCs have been marketed as ASDs [7], the design of these formulations poses the following questions:

- How to choose the appropriate polymer and its optimal concentration to ensure the physical stability of the drugs in the FDC?
- Is the stabilization mechanism attributable to drug-drug and drug-polymer intermolecular interactions?

Therefore, we propose an ASD design approach for drug combinations with the following steps (Figure 4):

1) The two APIs can interact and stabilize each other at a specific stoichiometry in the amorphous state. However, we will have one drug in "excess" (a fraction uninteracted) since the dose of the two APIs is unlikely to exactly match the above stoichiometry.
2) A polymer will complement and stabilize the amorphous system by interacting with the "excess" amorphous API.

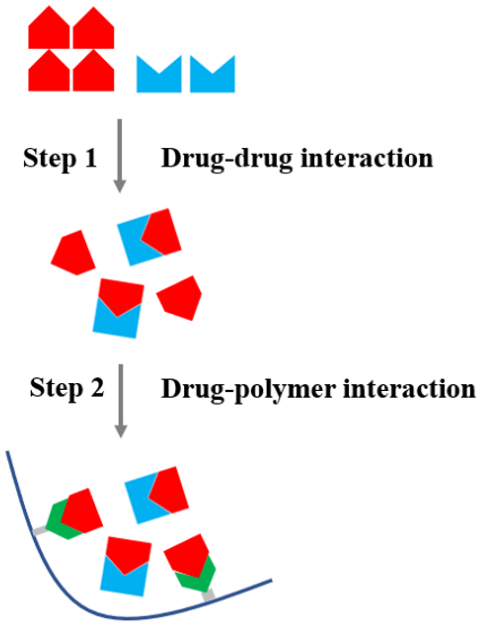

Figure 4. Schematic of the design approach for ternary ASD.

We hypothesize that the proposed drug-drug and drug-polymer interactions, by reducing molecular mobility, will enhance the physical stability of the ternary ASDs. The overall goal of our project was to develop a formulation platform strategy for the dissolution enhancement of two APIs in an ASD.

CHAPTER 2

INTRODUCTION

To enhance the solubility for poorly water-soluble drug combinations, an approach to design its ASD was proposed. The antibiotic combination of trimethoprim (TMP) and sulfamethoxazole (SMZ) was selected as the model system (Figure 5a). Clinically, the two drugs are used at SMZ:TMP weight ratio of 5:1. The common dose is 400 mg of SMZ and 80 mg of TMP. In addition to being a high-dose formulation (480 mg of APIs per tablet), there is a pronounced difference in the dose of the two APIs. This makes this combination a suitable and challenging model system for a multi-drug formulation. In order to check the practical usability of our approach, we reversed the weight ratio to 1:5 (SMZ:TMP) and examined the composition in detail (Figure 6). Thus, we aim to look at a wide weight ratio of drug combinations. SMZ is a weak acid with the pK_a of 5.6. The 5-methyl-3-isoxazole of SMZ is an electron-withdrawing group making the secondary amine an active proton donor. On the other hand, TMP is a weak base with a pK_a of 7.2 [17]. The interaction between the two to form a salt is documented [18]. In the first combination (SMZ:TMP = 5:1, w/w), since the acidic API is in excess, a basic polymer will be used to stabilize the system. An aminoalkyl methacrylate copolymer with a pK_a of 9.0 (Eudragit® EPO, EDE) was selected for this purpose (Figure 5a). The tertiary amine can act as a proton acceptor, interacting with acidic drugs via ionic interactions [19]. For the other composition (SMZ:TMP = 1:5, w/w), polyacrylic acid (PAA), an acidic polymer (pK_a = 4.5), was selected (Figure 5a). PAA can interact ionically with TMP and stabilize the system [20]. The proposed drug-drug and drug-polymer interactions are presented in Figure 5b. We have hypothesized that the above intermolecular interactions will physically stabilize the drugs in the ternary ASDs

and enhance drug dissolution. The intermolecular interactions were characterized using infrared spectroscopy (IR). The molecular mobility of the amorphous samples was determined by dielectric spectroscopy (DES). Differential scanning calorimetry (DSC) was used to determine the glass transition temperature (T_g) and crystallization onset temperature (T_c). Variable temperature X-ray diffractometry (XRD) and stability testing under accelerated conditions were carried out to study the physical stability. The dissolution performance of the ternary ASDs was evaluated under non-sink conditions.

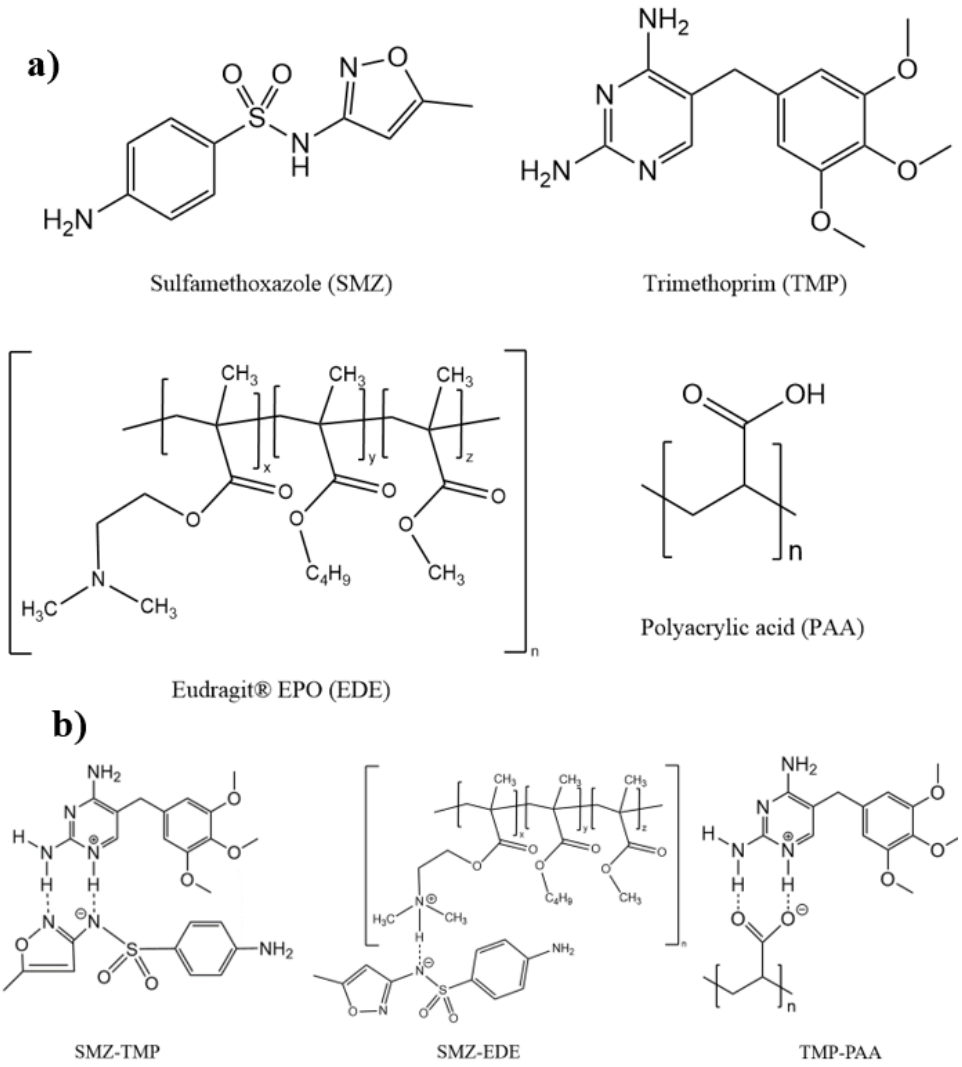

Figure 5. a) Chemical structures of SMZ, TMP, EDE (x:y:z = 2:1:1), and PAA. b) Proposed drug-drug and drug-polymer intermolecular interactions.

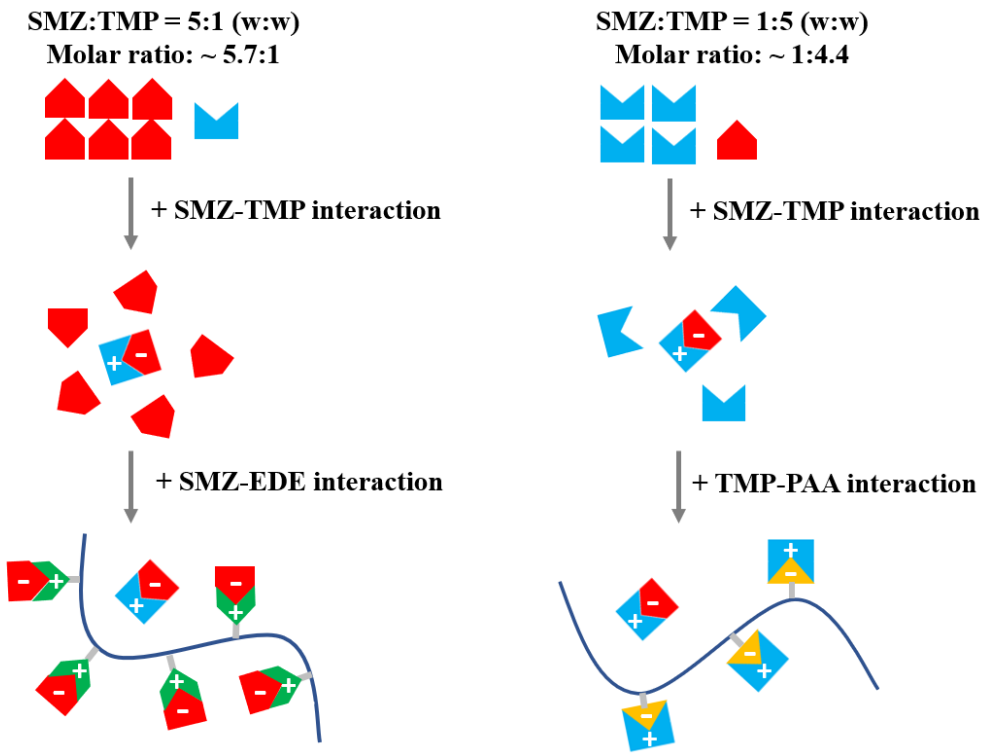

Figure 6. Schematic of the design approach for ternary ASD. Step 1: SMZ-TMP interaction in amorphous state. Step 2: introducing polymer to stabilize the excess component by drug-polymer interaction. The number of the drug molecules is determined by the molar ratios of the combinations, which are approximately 5.7:1 and 1:4.4 for the 5:1 and 1:5 (w/w) combinations.

MATERIALS AND METHODS

Materials

Sulfamethoxazole (SMZ) and polyacrylic acid (PAA) (Mw ≈ 1800) were purchased from Sigma-Aldrich (Missouri, USA). Trimethoprim (TMP) was purchased from Tokyo Chemical Industry (New Jersey, USA). Eudragit® EPO (EDE) was kindly donated by Evonik (New Jersey, USA). All the solvents and other chemicals were of analytical grade.

Sample preparation

Amorphous SMZ was prepared by melt quenching. The crystalline SMZ was heated to 170°C (about 5°C higher than the melting temperature), held for 5 min and quench cooled with liquid nitrogen. TMP, in light of its high crystallization propensity, could only be rendered amorphous by heating in the DSC. It was heated to 205°C, held for 5 minutes and quench cooled. The SMZ/TMP salt was prepared by dissolving SMZ and TMP in methanol at 1:1 molar ratio and slowly evaporating at room temperature.

Table 1. The composition of the designed ASDs.

	SMZ		TMP		Eudragit*		PAA		Mass ratio※
	mass (mg)	mole (mmol)	mass (mg)	mole (mmol)	mass (mg)	mole (mmol)#	mass (mg)	mole (mmol)#	
SMZ-EDE	500	1.97	-	-	356	0.99	-		0.58:0.42
SMZ-PAA	500	1.97	-	-	-	-	142	1.97	0.78:0.22
TMP-PAA	-	-	500	1.72	-	-	124	1.72	0.80:0.20
TMP-EDE	-	-	500	1.72	296	0.86	-	-	0.63:0.37
SMZTMP (5:1)-EDE	500	1.97	100	0.34	280	0.82	-	-	0.56:0.11:0.33
SMZTMP (1:5)-PAA	100	0.39	500	1.72	-	-	96	1.33	0.14:0.72:0.14

Moles of the monomer

* Because the molar ratio of dimethylaminoethyl methacrylate, butyl methacrylate, and methyl methacrylate groups is 2:1:1 in a single monomer, one mole of EDE monomer is assumed to interact with two moles of SMZ.

※ The mass ratio of drug-polymer or drug-drug-polymer ASDs.

The compositions of the binary and ternary ASDs are presented in Table 1. In general, the polymer content is determined based on the drug-monomer molar ratio for the proposed drug-polymer interactions. Binary and ternary ASDs were prepared by rotary evaporation. Drugs and polymers were dissolved in methanol at calculated ratios. The solvent was

evaporated at 60℃ under reduced pressure (IKA-HB10 digital system rotary evaporator, Werke GmbH and Co., Staufen, Germany). The samples were stored in a vacuum dryer at room temperature for two days to remove residual solvent. In order to prepare SMZ/TMP coamorphous samples, in total 600 mg SMZ and TMP crystalline APIs at the ratio of either 5:1 or 1:5 (w/w) were mixed by a mortar and pestle. The physical mixture was then melted at 205℃, held for 1 min, and rapidly quenched with liquid nitrogen. The prepared amorphous samples were stored at – 20℃ in airtight containers with anhydrous calcium sulfate for further use.

Differential Scanning Calorimetry

A differential scanning calorimeter (TA instrument Q2000, DE, USA) with a refrigerated cooling accessory was used. The instrument was calibrated with indium. About 5 – 10 mg of sample was heated at 10℃/min in hermetically crimped (T_{zero}) pans under nitrogen purge (50 mL/min). The glass transition temperature (T_g) and melting point (T_m) were determined at the midpoint of the transition. The crystallization onset temperature (T_c) was the onset of the transition.

Variable Temperature X-ray Diffractometry

Amorphous APIs, coamorphous SMZ-TMP systems, and ASDs were characterized by an X-ray diffractometer (D8 ADVANCE, Bruker AXS, WI, USA) equipped with a variable temperature stage (TTK 450; Anton Paar, Graz-Straβang, Austria) and a Si strip one-dimensional detector (LynxEye; Bruker AXS, Wisconsin, USA). The heating rate was 10℃/min, and the sample was maintained under isothermal conditions during each XRD scan. The measurements were performed in 10℃ increments from room temperature to

170°C. Co K_α radiation (1.54 A, 35 kV × 45 mA) was used, and data were collected in the range of 5 – 35° 2θ and a 1 s dwell time. Accelerated studies were carried out under 40°C/75 % relative humidity (RH) and evaluated by XRD at specific time points.

Infrared Spectroscopy

The IR spectra of model drugs, polymers, physical mixtures (PM), and all the amorphous samples were obtained in a spectrometer (Vertex 70, Bruker, Ettlingen, Germany; equipped with a globar mid-IR source) using an attenuated total reflectance (ATR) accessory (single reflection germanium crystal) and a DLaTGS detector. 64 scans were obtained in the range of 4000 – 40 cm^{-1} at a resolution of 4 cm^{-1}. All the measurements were carried out at approximately 25% RH.

Dielectric Spectroscopy

A dielectric spectrometer (Novocontrol Alpha-AK high-performance frequency analyzer, Novocontrol Technologies, Germany) equipped with a temperature control was used to measure the molecular mobility ranging from 40 to 140°C in steps of 5°C in the frequency range of 10^{-2} to 10^6 Hz. The experiments were carried out as a function of frequency at a fixed temperature. The high conductivity and electrode polarization significantly contributed to the dielectric loss spectra, complicating the relaxation time calculation. Therefore, the α-relaxation time of all the amorphous samples was obtained using a modified Havilak-Negami model function with an additional term (Eq. 1).

$$\varepsilon^*(\omega)=\varepsilon_\infty+\frac{\Delta\varepsilon}{(1+(i\omega\tau_{HN})^{\alpha})^{\gamma}}+\frac{\sigma_0}{i\omega\varepsilon_0}+A\omega^{-n} \quad \text{Eq. 1}$$

where ε_0 is the free space dielectric constant, ε_∞ is the high-frequency dielectric constant, $\sigma_0/i(\omega\varepsilon_0)$ is the dielectric loss contribution due to the dc conductivity (σ_0). A power-law dependence $A\omega^{-n}$ described the electrode polarization contribution to the real part of the dielectric constant, where A is the strength of the electrode polarization and n is the exponent. Havriliak-Negami (HN) function (2nd term of Eq.1) is used to model the relaxation process, where $\Delta\varepsilon$ is the dielectric strength of the α-relaxation process, τ_{HN} is the HN relaxation time and, α and γ are the shape parameters that determine the symmetric and asymmetric broadening of dielectric loss peak. Eq. 2 is applied to derive τ_α from the HN parameters [21].

$$\tau_\alpha = \tau_{\mathrm{HN}} \left[sin\left(\frac{\alpha\pi}{2+2\gamma}\right)\right]^{-1/\alpha} \left[sin(\frac{\alpha\gamma\pi}{2+2\pi})\right]^{1/\alpha} \quad \text{Eq. 2}$$

The temperature dependence of the α-relaxation time (τ_α) was analyzed using the Vogel−Fulcher−Tamman (VFT) equation:

$$\tau_\alpha = \tau_0 \exp\left(\frac{\mathrm{DT_0}}{\mathrm{T}-\mathrm{T_0}}\right) \quad \text{Eq. 3}$$

where τ_0 is the relaxation time constant for unrestricted materials (~ 10^{-14} s), T_0 is the Kauzman or zero mobility temperature, and D is the strength parameter. The τ value is extended to 100 s using the VFT parameters and the temperature at which τ_α = 100 s is assumed as the dielectric T_g.

High-performance liquid chromatography

A high-performance liquid chromatography (HPLC) method was developed to analyze the aliquots after diluting with the mobile phase. The concentrations of SMZ and TMP were

quantified using a YMC ODS-AQ column (C18, 4.6 μm × 250 mm, S-10 μm packing, column temperature: 25°C) at a flow rate of 2 mL/min with 5 μL of injection under the wavelength at 254 nm. The mobile phase is a water:acetonitrile:triethylamine = 69:30:1 (v/v/v). Linear regression between peak area and concentration showed $r^2 > 0.999$ for SMZ and TMP.

Solubility measurement

The solubility of SMZ and TMP at pH 1.2 and 6.8 are determined by equilibrating "as is" API powder at 37°C using a shaker. After filtration using 0.22 μm filter, the concentration was measured using HPLC.

Dissolution

A USP type II dissolution apparatus (Varian 705 DS, Agilent Technologies, Santa Clara, CA) was used to evaluate the dissolution of the crystalline mixture SMZ: TMP at 5:1 (w/w) and 1:5 (w/w), SMZTMP (5:1)-EDE and SMZTMP (1:5)-PAA ASDs. Samples equivalent to 1.5 g SMZ + 0.3 g TMP and 0.7 g SMZ + 3.5 g TMP were respectively dispersed in 500 mL pH 1.2 and pH 6.8 dissolution medium at 37°C with a paddle speed of 100 rpm. Before the dissolution tests, the powder was passed through US no. 80 mesh. At predetermined time points, 0.5 mL aliquots were withdrawn and filtered through a PTFE syringe filter (0.22 μm). The drug concentration was determined using the above HPLC method.

RESULTS

Baseline Characterization

The XRD patterns of "as is" SMZ and TMP were in excellent agreement with the XRD patterns from Cambridge Structural Database (CSD, Refcode: SLFNMB01 and AMXBPM10) (Figure S1). The polymorphs of "as is" APIs are SMZ form I and TMP form I. The XRD pattern of the SMZ/TMP salt was also in excellent agreement with the pattern calculated from CSD (Figure S2). The residual solvent content, determined by TGA, was less than 1% in all cases. The XRD patterns of the amorphous samples were characterized by broad halos and no discernible XRD peaks (Figure 15 and S4).

Thermal Analysis

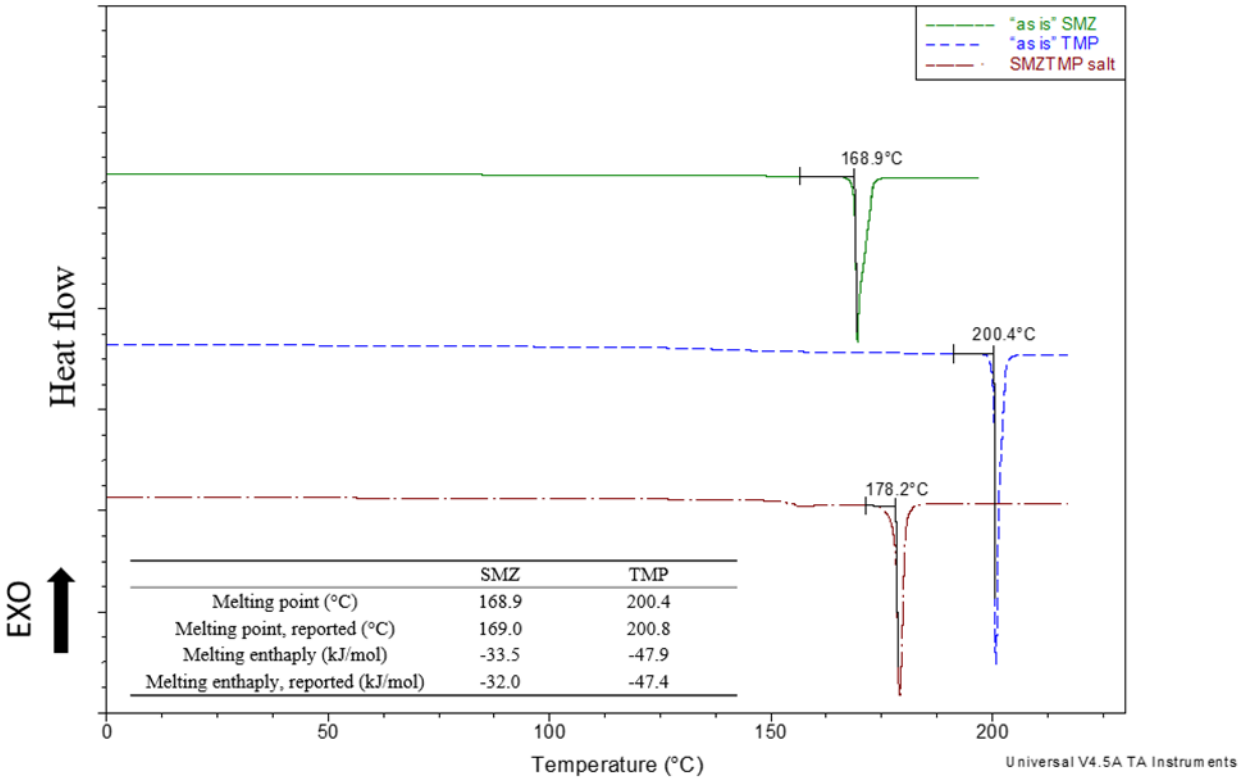

	SMZ	TMP
Melting point (°C)	168.9	200.4
Melting point, reported (°C)	169.0	200.8
Melting enthaply (kJ/mol)	-33.5	-47.9
Melting enthaply, reported (kJ/mol)	-32.0	-47.4

Figure 7. DSC heating curves of "as is" SMZ, TMP, and SMZ/TMP salt. The reported melting temperatures and enthalpy of fusion values were obtained from Ref. 22-23.

The DSC heating curves of "as is" crystalline SMZ and TMP revealed endotherms, respectively at 169°C and 200°C, attributable to melting (Figure 7). The melting temperatures and the enthalpy of fusion values were in good agreement with the literature [22-23]. The SMZ/TMP salt melted at 178°C (Figure 7).

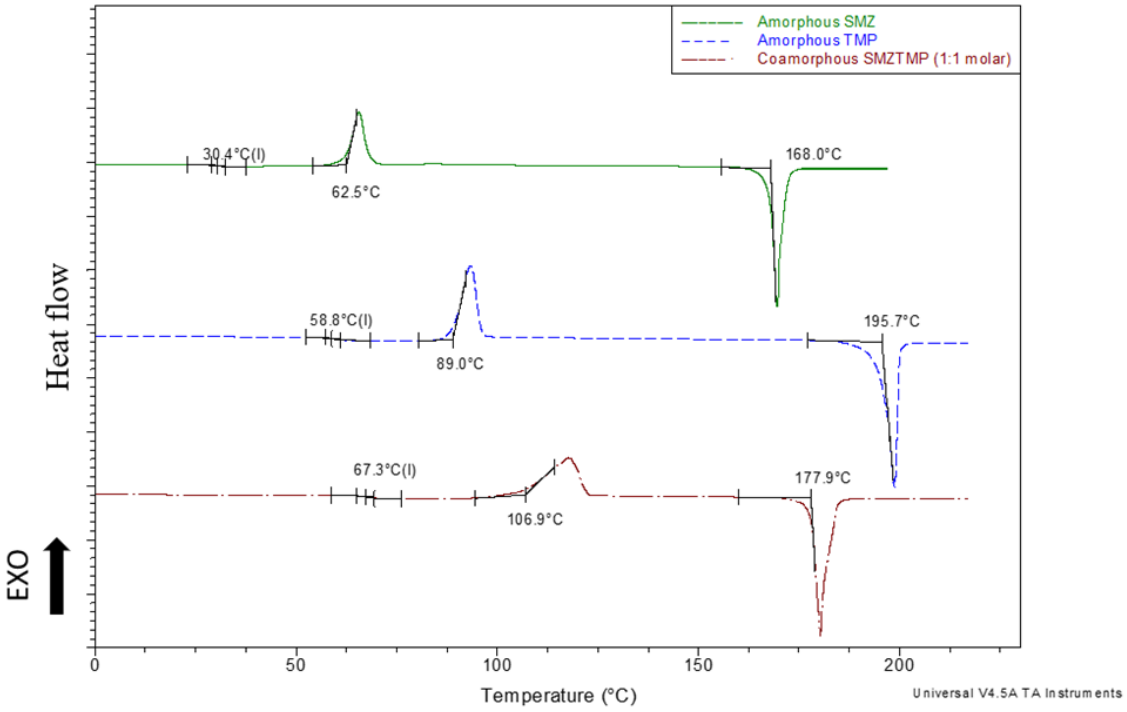

Figure 8. DSC heating curves of amorphous SMZ, TMP, and coamorphous SMZ/TMP (1:1, molar ratio).

The T_gs of amorphous SMZ and TMP, at 30°C and 59°C respectively were followed by crystallization at 63°C and 89°C, respectively (Figure 8). The T_g of the SMZ/TMP coamorphous phase was 67°C. This was followed by an exotherm at 107°C, attributable to crystallization, followed by an endotherm at 178°C (Figure 8). This endotherm is therefore ascribed to the melting of the SMZ/TMP salt. It is noteworthy that the crystallization

temperature of the 1:1 coamorphous salt (107°C) is higher than that of the individual amorphous APIs constituting the salt.

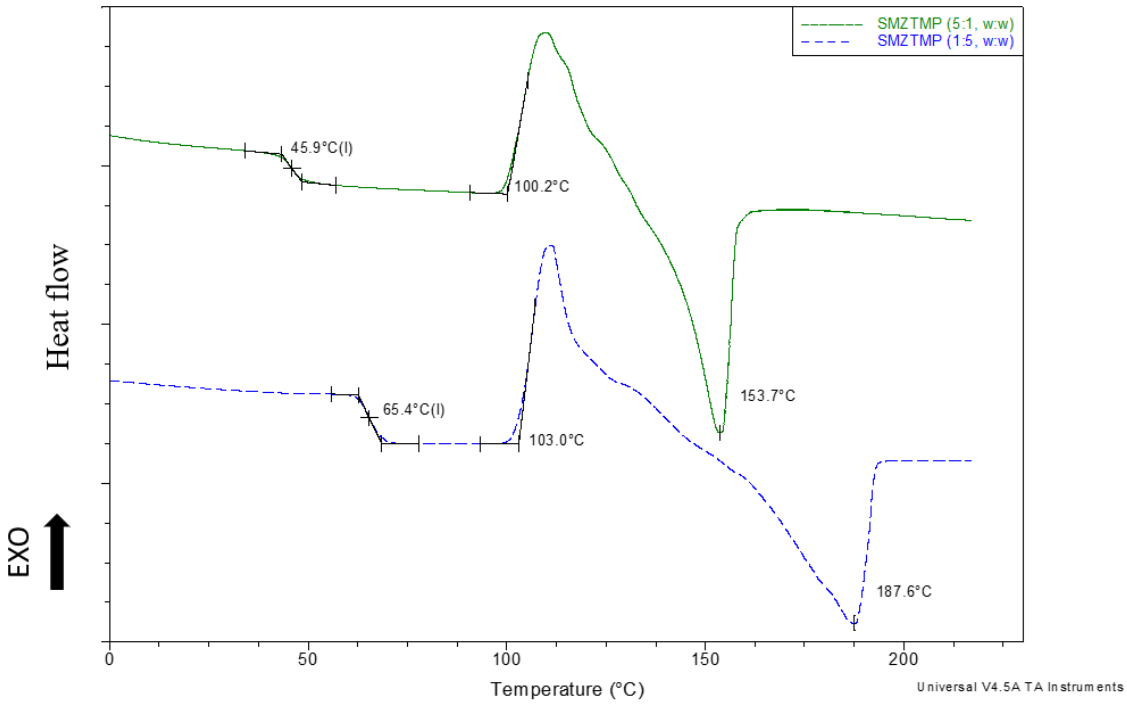

Figure 9. DSC heating curves of coamorphous SMZ/TMP at 5:1 and 1:5 (w/w).

However, the SMZ/TMP (5:1) is of interest from a practical point of view. As mentioned earlier, the SMZ/TMP (1:5) was evaluated to test the broad applicability of our approach. The T_g values of these compositions are given in Table 1. Compared with amorphous APIs, the crystallization onset temperatures of SMZ/TMP (5:1 and 1:5) coamorphous systems increased to 100°C and 103°C (Figure 9), indicating that the drug-drug interaction increased the resistance to crystallization and improved the physical stability of the coamorphous systems. The T_g of the (i) binary ASDs of SMZ and TMP, each in PAA and EDE, and (ii) the ternary ASDs are presented in Table 1. All these compositions reveal only one T_g, suggesting the formation of a single phase.

Table 2. Experimental T_gs, interaction parameters (q), and T_cs of amorphous drug-drug and drug-polymer systems and predicted and experimental T_gs of the ternary ASDs by the Kwei equations. The compositions of the above samples are given in Table 1.

Binary amorphous systems	T_g (°C)	q	T_c (°C)
SMZ	30		63
TMP	59		89
SMZ/TMP (5:1)	46	82	100
SMZ/TMP (1:5)	65	75	103
SMZ-EDE	60	68	ND
TMP-PAA	100	201	ND
SMZ-PAA	42	-33	107
TMP-EDE	59	-4	83
Ternary ASDs	T_g (°C), predicted		T_g (°C), experimental
SMZTMP (5:1)-EDE	61		62
SMZTMP (1:5)-PAA	90		91

ND: not detected

The Kwei equation provided an estimate of the strength of drug-drug and drug-polymer interactions. The equation provides a semi-quantitative measure of the effect of intermolecular interaction on the T_gs of polymer blends [24-25]. For binary systems (Eq. 4), the interaction parameter, q, can be obtained from the experimentally determined T_g and the known T_gs of the individual components (T_{g1} and T_{g2}) and their weight fractions (w_1 and w_2). In general, a significant positive q value represents strong intermolecular interaction, while a negative q value reflects a weak interaction.

$$T_g = \left(w_1 T_{g1} + w_2 T_{g2}\right) + q_{12} w_1 w_2 \qquad \text{Eq. 4}$$

The positive q values of the SMZ-TMP, SMZ-EDE, and TMP-PAA systems indicate strong intermolecular interactions (Table 2). The TMP-PAA interaction, in light of the large q value, is possibly the strongest. Our earlier study on TMP-PAA binary ASD confirmed an ionic interaction between the drug and polymer [20]. The positive q value also suggests a potentially strong interaction between SMZ and EDE. As a basic polymer, EDE is expected to ionically interact with acidic drugs. For example, the protonation of the tertiary nitrogen of EDE by the carboxylic acid group of indomethacin and naproxen was observed in their ASDs [26-27].

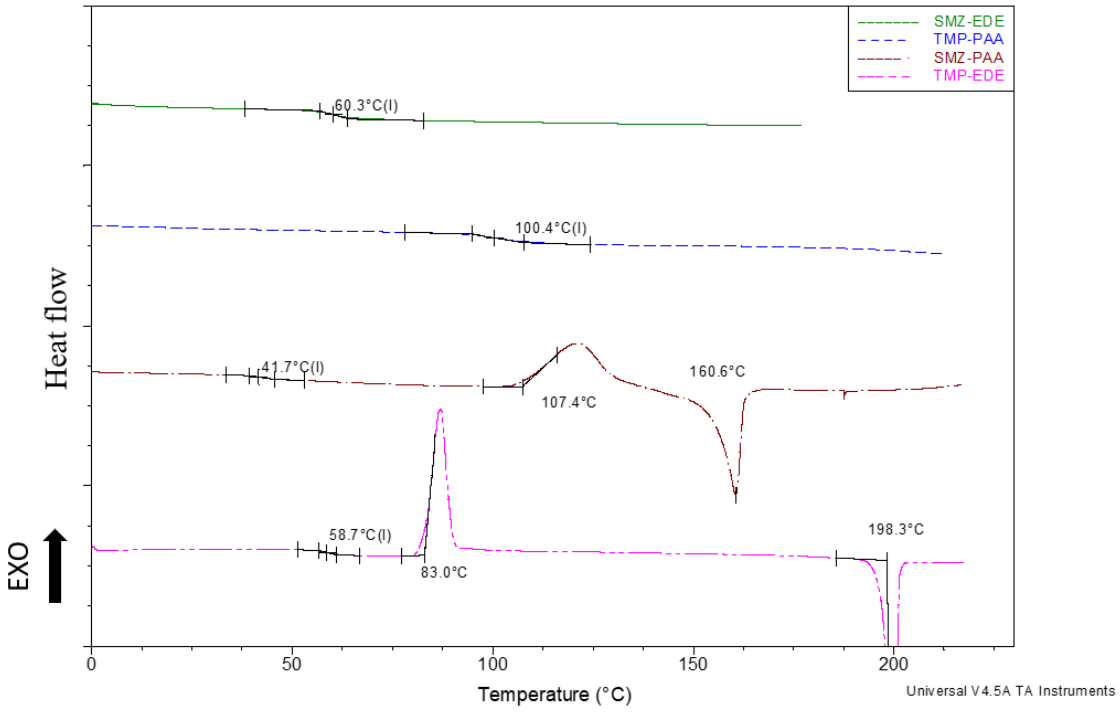

Figure 10. DSC heating curves of binary SMZ-EDE, TMP-PAA, SMZ-PAA, and TMP-EDE ASDs.

The DSC of SMZ-EDE and TMP-PAA ASDs, even when heated to 220°C, did not reveal drug crystallization reflecting the improved physical stability of the drug (Table 2, Figure

10). Besides, no crystallization exotherms were observed in the DSC of SMZ-EDE and TMP-PAA ASDs when heated to 220°C, which means those ASDs were physically stable upon heating. In contrast, based on the negative q values, the drug-polymer interactions in the SMZ-PAA and TMP-EDE binary ASDs were weak. This was reflected in the crystallization of SMZ and TMP at 83°C and 107°C, respectively (Table 2, Figure 10).

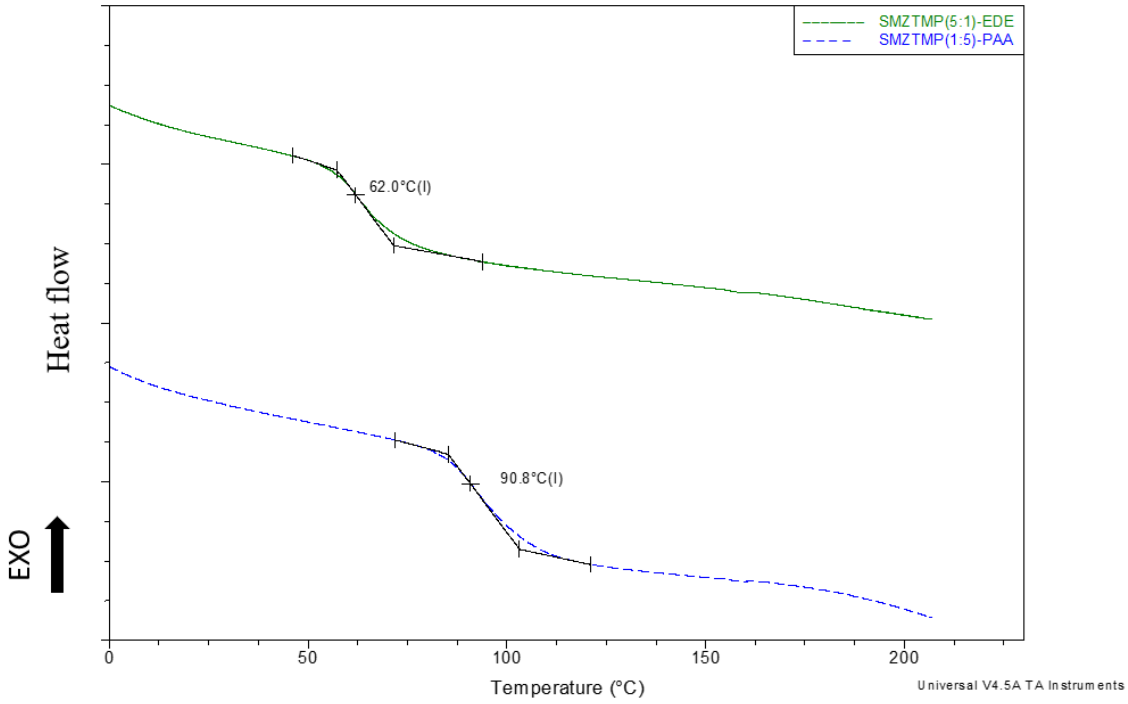

Figure 11. DSC heating curves of ternary SMZTMP (5:1)-EDE and SMZTMP (1:5)-PAA ASDs.

Once the q values were obtained for the binary systems, the modified Kwei equation (Eq. 5), enabled us to predict the T_gs of ternary systems. The weight fractions and T_gs of SMZ, TMP and polymer (either EDE or PAA) are w_1, w_2, w_3 and T_{g1}, T_{g2}, T_{g3}, respectively. Table 2 provides the q_{12} (SMZ-TMP), q_{23} (SMZ-polymer) and q_{13} (TMP-polymer) values.

$$T_g = \left(w_1 T_{g1} + w_2 T_{g2} + w_3 T_{g3}\right) + q_{12} w_1 w_2 + q_{23} w_2 w_3 + q_{13} w_1 w_3 \qquad \text{Eq. 5}$$

The experimental T_gs of the ternary ASDs were in excellent agreement with the predicted values (Table 2), strongly suggesting that the interactions in binary amorphous systems extend to the ternary ASDs. Added evidence of interaction was the absence of exotherm attributable to drug crystallization in the DSC curves of the two ternary ASDs (Figure 11). Thus, the thermal analysis strongly suggests the stabilization of ternary ASDs brought about by the drug-drug and drug-polymer interactions.

Intermolecular interactions

Intermolecular interactions are proposed to exist between: (i) SMZ-TMP, (ii) SMZ-EDE, and (iii) TMP-PAA.

SMZ-TMP interaction The crystal structure of the SMZ-TMP salt reveals a two-point interaction – (a) the SMZ N(2) hydrogen bonds with TMP N(7) and (b) TMP N(1) is protonated by the secondary amine SMZ N(7) (Figure 12) [18].

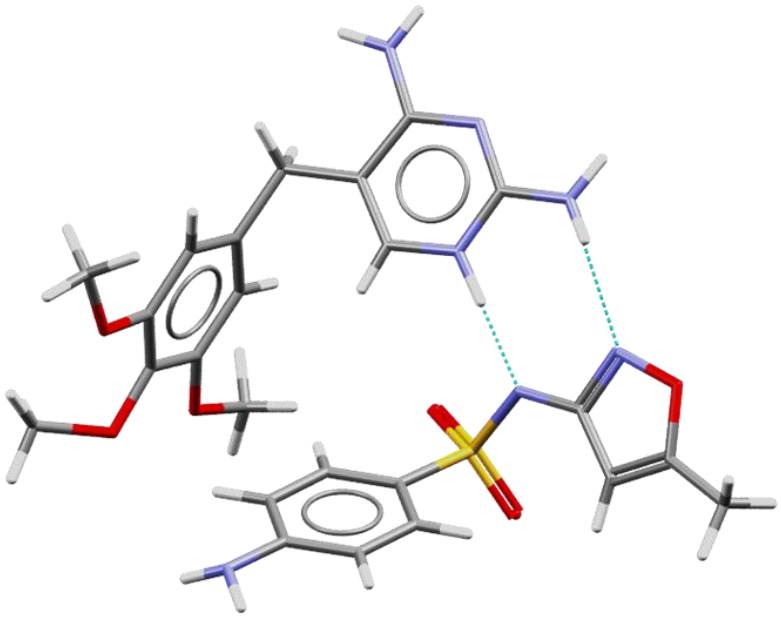

Figure 12. The intermolecular interaction presents in the SMZ/TMP salt single crystal data (CSD Refcode: SMZTMP01).

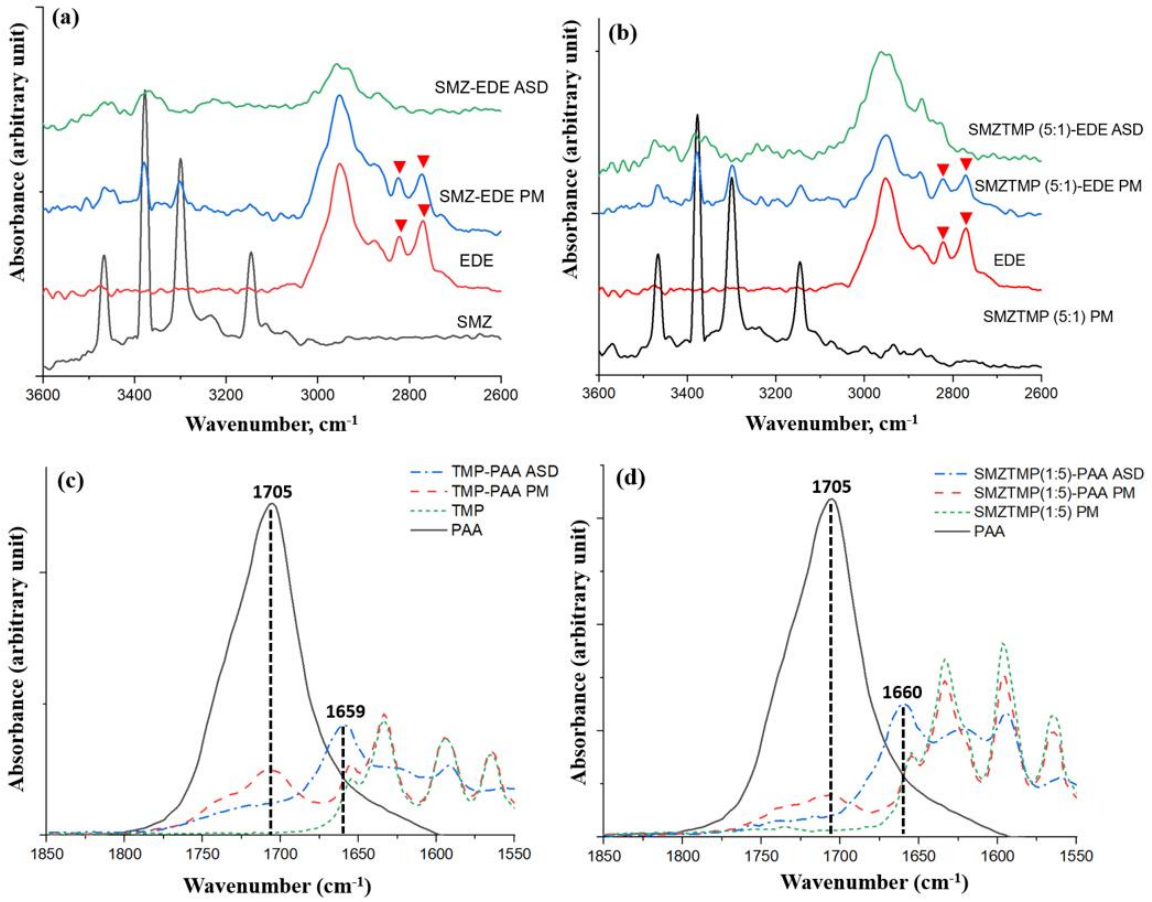

Figure 13. IR spectra of (a) "as is" SMZ, EDE and their physical mixture and ASD (bottom to the top); (b) SMZ-TMP crystalline mixture (5:1, w/w), EDE and their physical mixture and ASD (bottom to top); (c) "as is" PAA, TMP and their physical mixture and ASD, (d) PAA, SMZ-TMP crystalline mixture (1:5, w/w), and their physical mixture and ASD. The compositions of the above samples are given in Table 1.

SMZ-EDE interaction The $\triangle pK_a$ of 3.4 between the conjugate acid of EDE (pK_a = 9.0) and SMZ (pK_a = 5.6) reveals the potential for ionic interaction between the drug and polymer. The drug-polymer interaction was further investigated using IR spectroscopy. In the IR spectra of "as is" EDE and SMZ-EDE physical mixture, the peak at 2950 cm^{-1} is attributed to C – H stretching and the dimethylamine group of "as is" EDE reveals peaks at 2821 and 2772 cm^{-1} (Figure 13a and 13b, highlighted with red reverse triangles) [27]. For

the crystalline SMZ and SMZ-EDE physical mixture, the peaks between 3500 to 3000 cm^{-1} represent the N – H stretching of the amino groups (Figure 13a and 13b). In the binary and ternary ASD, the secondary amine of SMZ possibly protonates the tertiary nitrogen of EDE, causing the disappearance of the two peaks at 2821 and 2772 cm^{-1} (Figure 13a and 13b). This was confirmed by the absence of these characteristic peaks in the IR spectrum of the EDE-hydrochloride polymer salt, indicating the tertiary amine protonation (Figure S3) [28].

TMP-PAA interaction The intense peak at 1705 cm^{-1}, ascribed to the C = O stretching of the carboxylic acid, was observed in the IR spectra of PAA and TMP-PAA physical mixture (Figure 13c). On forming an ASD, the carboxylic acid deprotonates and the C = O stretching peak shifts to 1659 cm^{-1}. We had earlier documented this ionic interaction between PAA and TMP [20]. In the ternary ASD, a similar peak shift from 1705 cm^{-1} to 1660 cm^{-1} was observed, indicating the continued existence of the ionic interaction (Figure 13d).

Molecular Mobility

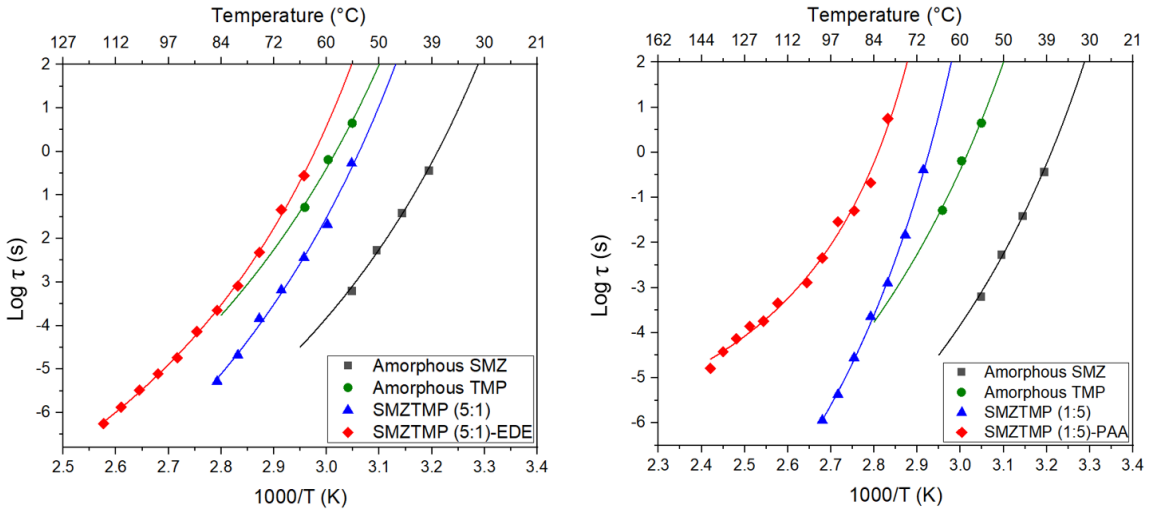

Figure 14. Temperature dependence of α-relaxation times (τ) in amorphous APIs: SMZ (black) and TMP (green), SMZ/TMP coamorphous systems (blue), and ternary ASDs (red)

for the 1:5 (panel a) and 5:1 (panel b) combinations in weight ratios. The data, fitted using the VFT equation, was extended to τ_α = 100 s. The corresponding temperature is considered the dielectric T_g.

The α-relaxation time, determined by dielectric spectroscopy, is a direct measure of molecular mobility. Figure 14 provides the temperature dependence of α-relaxation time (τ) in the supercooled state of amorphous APIs, SMZ/TMP coamorphous systems, and ternary ASDs. The temperature dependence of τ followed the Vogel-Fulcher-Tammann (VFT) relationship. In the entire temperature range studied, each sample was characterized by a single relaxation time. This confirms the conclusion from DSC of the formation of a single amorphous phase (no phase separation).

We will compare the behavior of the different compositions in the context of the major drug component. The SMZ/TMP (5:1) coamorphous system, compared with amorphous SMZ, shows about 3 orders of magnitude reduction in molecular mobility (Figure 14a). EDE further immobilizes the system and results in approximately an additional 2 orders of magnitude decrease in molecular mobility. For the SMZ/TMP (1:5) system (Figure 14b), the coamorphization caused ~ 1 order of magnitude increase in α-relaxation time when compared with amorphous TMP. The addition of PAA caused a pronounced and further increase in α-relaxation time of ~ 4 orders of magnitude. The above discussion, for both ratios (5:1 and 1:5), is somewhat of a generalization and is not valid for the entire temperature range. A previous study proved that strong intermolecular interactions in KTZ-organic acids coamorphous systems resulted in a significant reduction in molecular mobility when compared with amorphous KTZ. The addition of PVP further stabilized the ternary ASDs without interfering with the drug-excipient interactions [29]. In our case, while

both drug-drug and drug-polymer interactions "immobilize" the drugs, the general rank order in terms of molecular mobility is: ternary ASDs < coamorphous systems < amorphous APIs.

Physical Stability

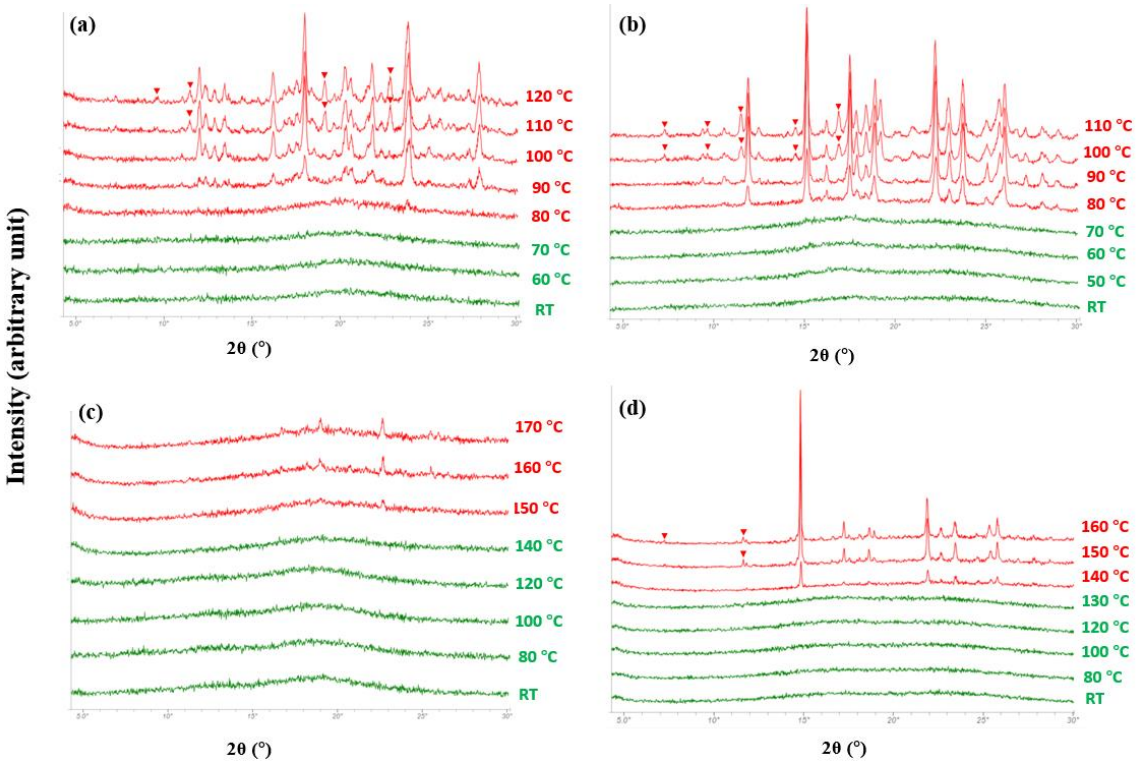

Figure 15. Variable temperature XRD patterns of (a) SMZ/TMP (5:1) and (b) SMZ/TMP (1:5) coamorphous systems, (c) SMZTMP (5:1)-EDE and (d) SMZTMP (1:5)-PAA ternary ASDs. The diffraction peaks of the SMZ/TMP salt are highlighted with red revert triangles.

While DSC heating curves contained exotherms attributable to crystallization, variable temperature XRD enabled direct identification of the crystallizing phases. Both amorphous SMZ and TMP are unstable with a high crystallization propensity. Upon heating, amorphous SMZ recrystallized at ~ 40°C (Figure S4). On a reasonable scale (~ 100 mg), TMP could not be rendered amorphous by melt quenching. Binary coamorphous systems

recrystallize either into individual components or their relevant salt/cocrystal. For instance, the carbamazepine-benzoic acid coamorphous system recrystallized as a cocrystal while carbamazepine-succinic acid coamorphous system recrystallized into individual components [30]. In case of the SMZ/TMP (5:1) coamorphous system, crystalline SMZ first appeared at 80°C, followed by SMZ/TMP salt crystallized at 110°C (Figure 15a). Relatively, in the SMZ/TMP (1:5) coamorphous system, TMP first crystallized at 80°C and the salt crystallized at 100°C (Figure 15b). The addition of EDE and PAA significantly enhanced the physical stability (Figure 15c and 15d). In case of the PAA ASD, TMP and the SMZ/TMP salt crystallized at 140°C and 150°C, respectively. In the ternary EDE ASD, while a few low intensity peaks appeared at ~ 150°C, the crystallizing phase(s) could not be unambiguously identified.

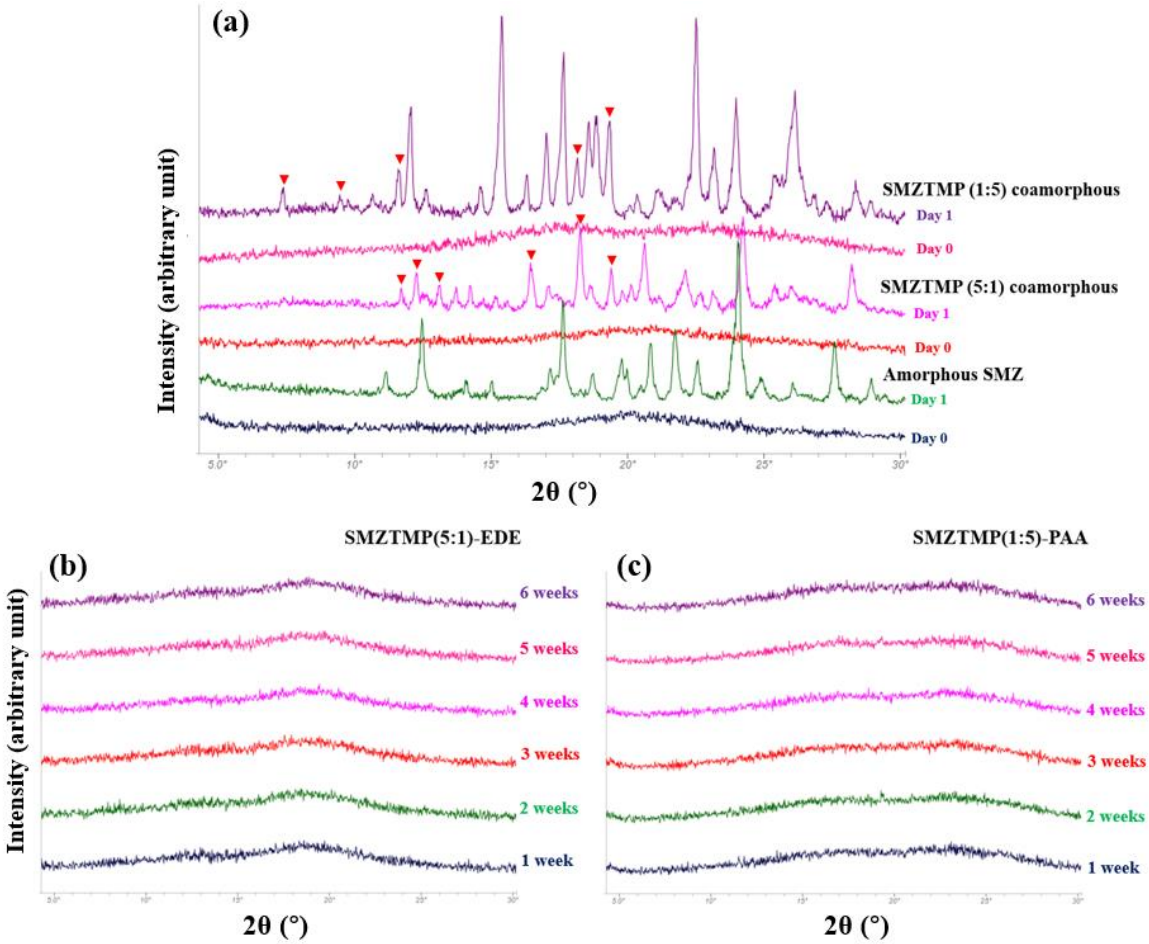

Figure 16. XRD results of (a) amorphous SMZ and coamorphous systems, (b) ternary EDE ASD, and (c) ternary PAA ASD after storage at 40°C/75% RH. The diffraction peaks of the SMZ/TMP salt are highlighted with red revert triangles.

The ternary ASDs were stable for at least 6 weeks at 40°C/75% RH. However, the amorphous SMZ and the SMZ/TMP coamorphous systems crystallized after storage for 24 hours (Figure 16). The XRD results confirm the rank ordering of stability: ternary ASDs > coamorphous systems > amorphous APIs.

According to the intermolecular interactions and DES results, the drug-drug interactions improve the stability of the SMZ/TMP coamorphous systems. The strong drug-polymer

interaction further stabilized the ternary ASD by significantly reducing the molecular mobility.

Dissolution

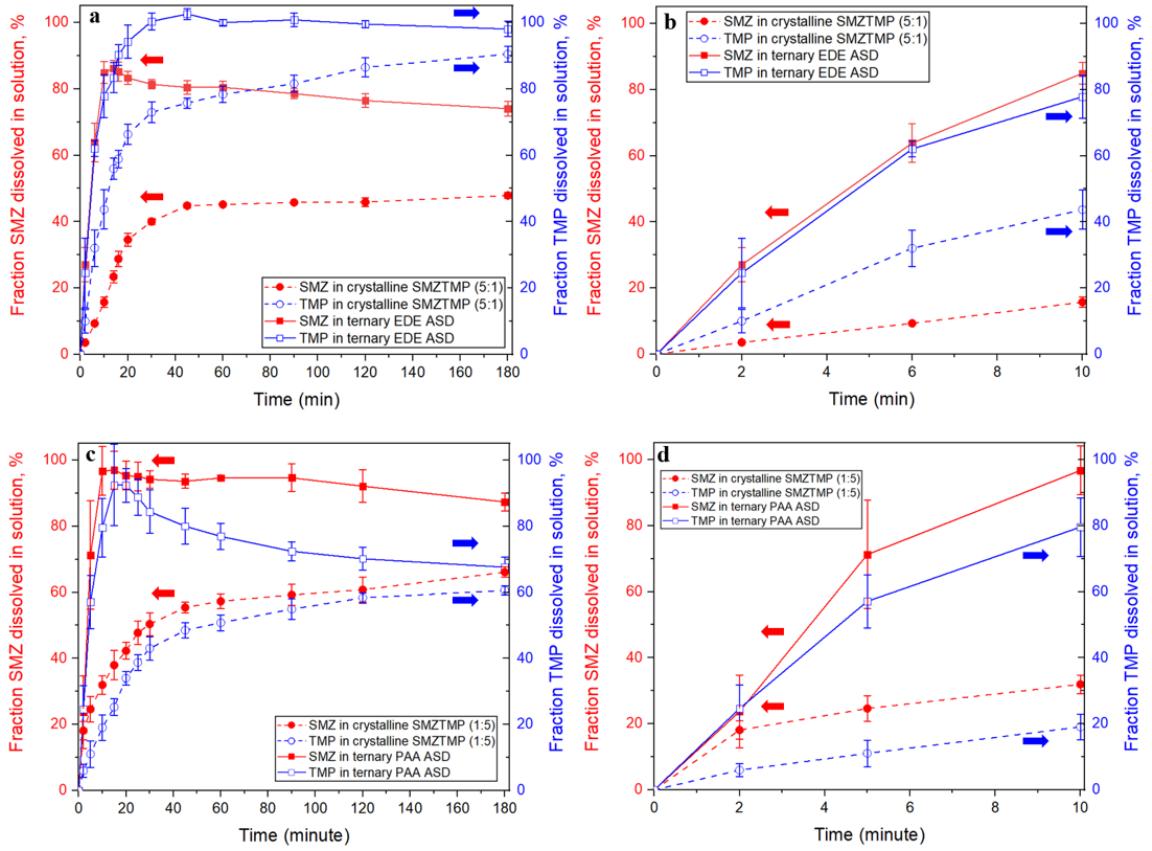

Figure 17. Dissolution profiles of (a) SMZ/TMP (5:1, w/w) crystalline mixture and SMZTMP (5:1)-EDE ASD at pH 1.2 and (c) SMZ/TMP (1:5, w/w) crystalline mixture, and SMZTMP (1:5)-PAA ASD at pH 6.8. Panels (b) and (d) are the expanded profiles (initial dissolution; up to 10 minutes) of panels (a) and (c), respectively. The left and right y-axis provide the dissolved fraction (%) of SMZ and TMP, respectively. At the end of the dissolution experiment, the pH change was ≤ 0.3 pH units.

Table 3. Dissolution results (37°C) of crystalline SMZ-TMP mixtures and ternary ASDs.

SMZ:TMP = 5:1 (w/w)	T_{max} (min)	C_{max} (μg/mL)	AUC (0→10) (μg/mL min)	AUC ratio[#] (mean)
Crystalline SMZ	180	732 ± 13	1193 ± 90	1
SMZ in EDE ASD	14	1292 ± 36	7594 ± 679	6.4
Crystalline TMP	180	271 ± 7	737 ± 134	1
TMP in EDE ASD	30	307 ± 8	1432 ± 163	1.9
SMZ:TMP = 1:5 (w/w)	T_{max} (min)	C_{max} (μg/mL)	AUC (0→10) (μg/mL min)	AUC ratio[#] (mean)
Crystalline SMZ	180	727 ± 17	2460 ± 325	1
SMZ in PAA ASD	15	1067 ± 56	6447 ± 1310	2.6
Crystalline TMP	180	3332 ± 76	5874 ± 1678	1
TMP in PAA ASD	15	5085 ± 316	26883 ± 3953	4.6

[#] $[AUC_{(0\rightarrow10\ min),\ ASD}]/[AUC_{(0\rightarrow10\ min),\ crystalline\ API}]$

The dissolution profiles of SMZ and TMP, from crystalline mixtures and the ternary ASDs, are provided in Figure 17. The SMZ to TMP weight ratios were 5:1 (Figure 17a and 17b) and 1:5 (Figure 17c and 17d). In the SMZ/TMP 5:1 composition, based on the T_{max} and C_{max} values, SMZ in the EDE ASD shows a faster dissolution rate and much higher C_{max} than the crystalline SMZ (Figure 17a and Table 3). The difference was much less pronounced for TMP. The area under the curve (AUC) values obtained from the concentration−time profiles were used to compare their dissolution performance (Table 3). According to the initial dissolution profile (first 10 min; Figure 17b), the AUCs of SMZ and TMP in the EDE ASD are 6.4 and 1.9 times that of the corresponding crystalline APIs. At this time, ~ 80% of the SMZ in the ASD had dissolved, but only 20% of the crystalline SMZ. The rapid dissolution from the ASD was followed by a small and gradual decrease

in SMZ concentration (Figure 17a). However, the crystalline SMZ continued to dissolve until 180 min. Based on the aqueous solubility of TMP at pH 1.2 (5.6 mg/mL; 37°C), all the added TMP (300 mg) will be completely released in the dissolution medium. At 3 hours, ~ 90% of the TMP has dissolved. However, amorphization resulted in a more rapid release, specifically during the early stages (Figure 17b). In case of SMZ/TMP 1:5 (w/w), both the APIs dissolved rapidly from the ASD. Based on the initial dissolution profiles (first 10 min; Figure 17d), the AUCs of SMZ and TMP in the PAA ASD are respectively 2.6 and 4.6 times that of the crystalline APIs (Table 3). At this time, substantial (≥ 80%) dissolution of the drugs in the PAA ASD was observed (Figure 17d). Over a longer time period, TMP crystallized from solution, while in light of SMP, this appeared to occur at a very slow rate (Figure 17c and Table 3). In both ternary ASDs, the residual solid at the end of the dissolution was identified by XRD to be a mixture of the SMZ/TMP salt and the component present in excess (Figure S5).

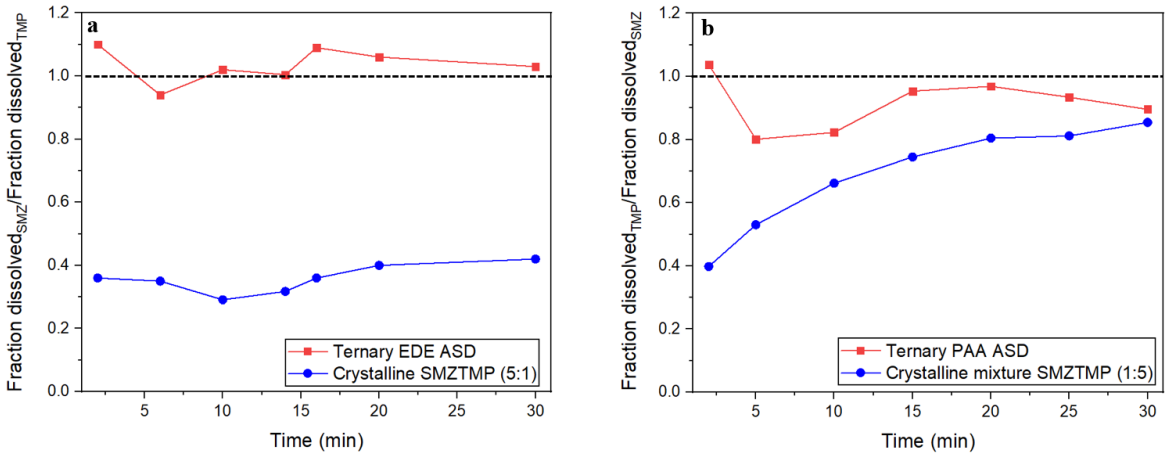

Figure 18. Average dissolved fraction ratios of SMZ/TMP and TMP/SMZ for ternary ASDs (red curves) and crystalline mixtures (blue curves) during dissolution at pH 1.2 (panel a) and pH 6.8 (panel b). The black dash lines represent the ratio when the same fractions of SMZ and TMP are dissolved (synchronized released).

A unique attribute of the ASDs was the synchronized release of the two APIs. This is evident from a plot of the ratios of the dissolved fractions of the two APIs as a function of time (Figure 18). The ratio is close to unity, revealing that, at any given time, approximately the same fraction of the two APIs was released. This plot was restricted to the first 30 minutes since at later time points, the drop in concentration due to crystallization became pronounced (evident in Figures 17a and 17c). For the crystalline physical mixtures, the higher solubility of TMP results in the ratio being << 1. This effect is observed irrespective of pH. However, SMZ/TMP (1:5) crystalline mixture, at pH 6.8, the ratio approaches 1 as dissolution progresses.

DISCUSSION

Our project proposes an ASD formulation development strategy for FDCs based on drug-drug and drug-polymer interactions. We have characterized the ionic drug-polymer interactions using IR spectroscopy (Figure 13). Due to the skewed ratio of the two APIs in a combination, we were not able to successfully distinguish the drug-drug interactions in the ternary ASDs. However, the stabilization effect of the drug-drug intermolecular interactions was indirectly revealed in the thermal, molecular mobility, and physical stability studies (Table 2, Figures 14 and 15). Although individual amorphous APIs had a high crystallization propensity, the drug-drug interaction in the SMZ/TMP coamorphous systems resulted in a pronounced reduction in molecular mobility and improved the physical stability. From the variable temperature XRD study (Figure 15), it is evident that the excess API first crystallized, followed by the SMZ/TMP salt, indicating that the salt has a lower crystallization propensity than the amorphous APIs. Thus, the intermolecular

interaction in the amorphous state is manifested in the phases crystallizing from the ASDs. For example, the intermolecular interactions between ketoconazole and dicarboxylic acids in salts also stabilized the ketoconazole-organic acid coamorphous systems [31]. Unfortunately, the SMZ/TMP coamorphous systems did not exhibit adequate stability and recrystallized after 24 h at 40°C/75% RH (Figure 16). Therefore, depending on the proportions of the two drugs in the formulation, either EDE or PAA was added and the ASD was fabricated. The polymer selection was based on its potential for interaction with API. The addition of polymers further immobilized the system and significantly improved the physical stability (Figure 15 and 16).

In addition to the enhanced dissolution of the ternary ASDs, we also observed unique synchronized release profiles for the two APIs. In the crystalline physical mixture of the two APIs, the more soluble component tends to dissolve faster, possibly in an unbalanced release. The measured solubility of SMZ and TMP are 1.5 mg/mL and 5.6 mg/mL at pH 1.2, and 1.8 mg/mL and 2.8 mg/mL at pH 6.8, respectively, which means TMP is expected to dissolve faster than SMZ irrespective of pH. In the SMZ/TMP (5:1) crystalline mixture, the unbalanced release of TMP is quite pronounced at pH 1.2. Thus, the ratios of the dissolved fractions of the two APIs are << 1 (Figure 18a). However, the ratio approaches to 1 as dissolution progresses for SMZ/TMP (1:5) crystalline mixture at pH 6.8 (Figure 18b). This may be attributed to the closer solubility values of the two APIs at pH 6.8 than at pH 1.2. The ratios of the dissolved fractions of the two APIs in the ASDs are close to unity, indicating a more synchronized release profile (Figure 18). The formation of a single phase ternary ASD due to drug-drug and drug-polymer interactions possibly resulted in the simultaneous dissolution of the amorphous APIs. A similar phenomenon has been observed

in 1:1 coamorphous systems that revealed a synchronized release profile, while the APIs in a physical mixture dissolved independently [32-33]. The synchronized release may be a desirable attribute when two drugs exert synergistic effects [34].

According to the dissolution results, the designed ternary ASDs have the following advantages: 1) improved physical stability, 2) enhanced dissolution, and 3) synchronized release.

CONCLUSION

An ASD design strategy for drug combinations has been developed by exploiting drug-drug and drug-polymer interactions. The antibiotic combination of SMZ and TMP was employed as the model system. The interaction between the two drugs provided the first avenue of amorphous phase stabilization. The basic polymer EDE was used to stabilize the "excess" SMZ in ternary SMZ/TMP (5:1) ASDs. Likewise, the acidic polymer PAA was used to stabilize the excess TMP in ternary SMZ/TMP (1:5) ASDs. These interactions, by reducing molecular mobility, improved the physical stability of the ASDs. In addition to the enhanced dissolution, the ternary ASDs manifested synchronized dissolution profiles. By enhancing physical stability and dissolution, the proposed ASD design approach provided a rational way for the formulation development of poorly soluble drug combinations.

APPENDIX

Figures S1 to S5 included in this section

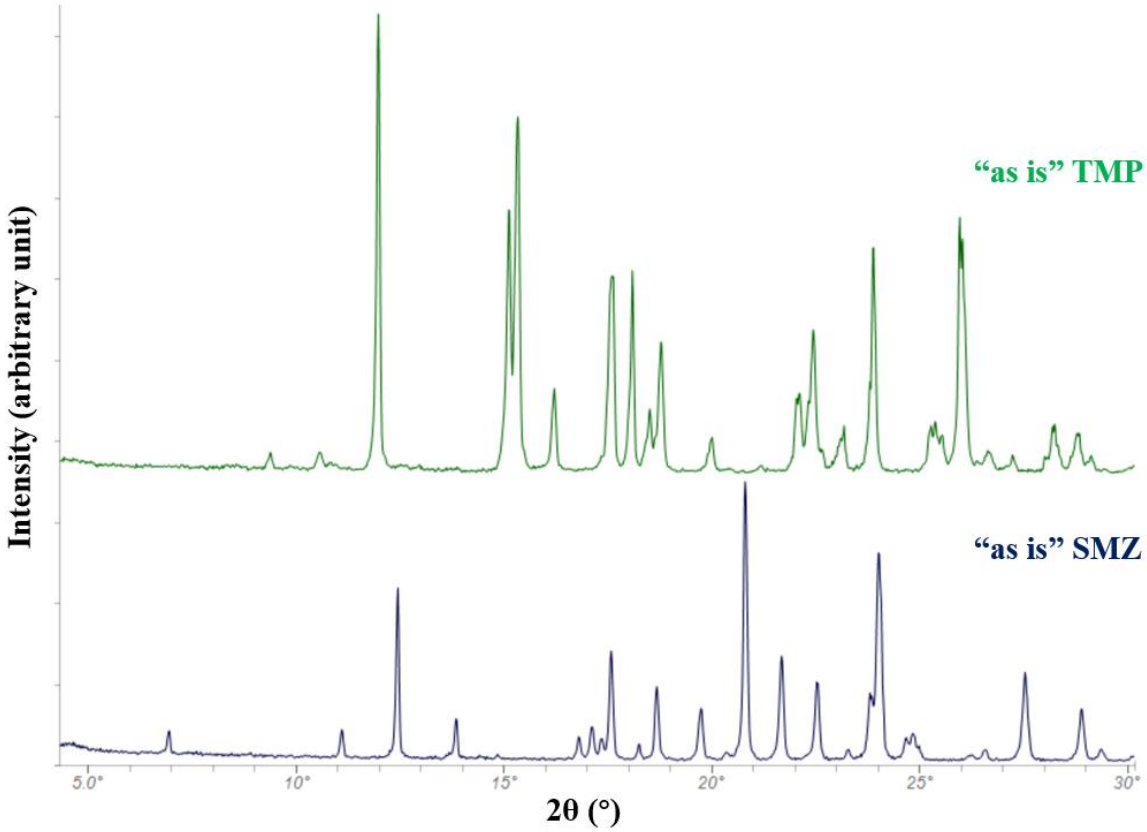

Figure S1. XRD patterns of "as is" SMZ and TMP.

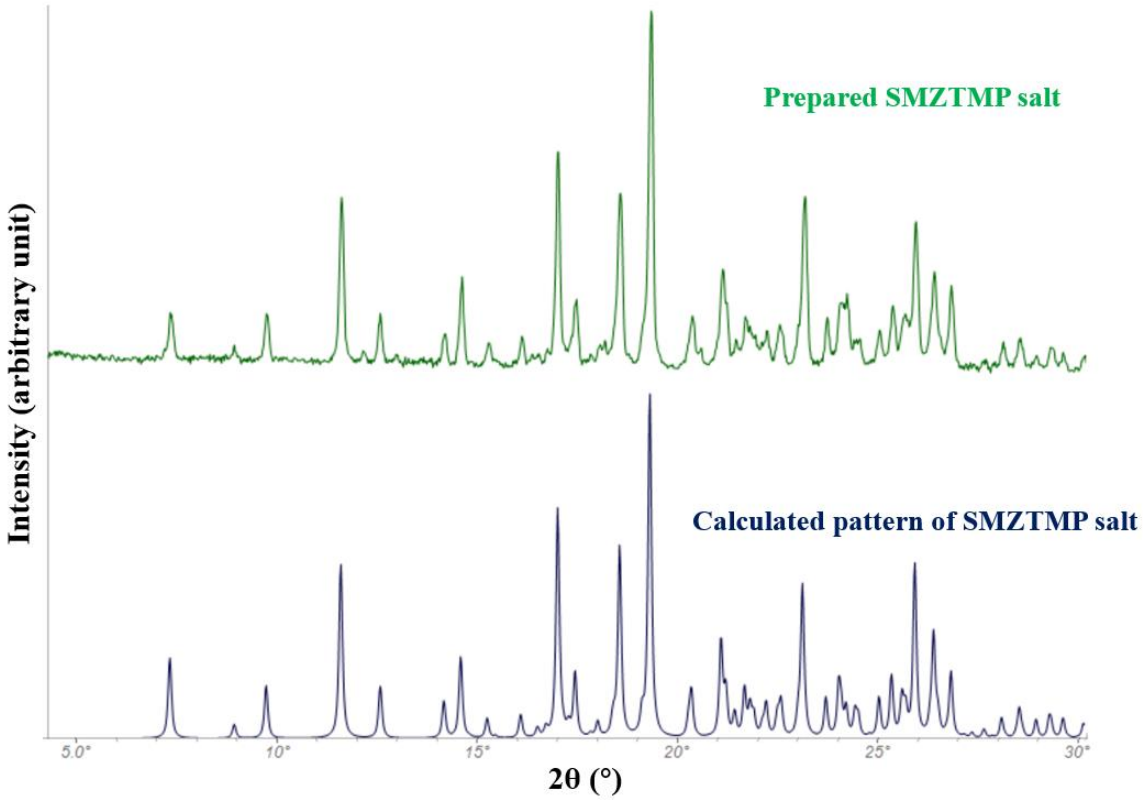

Figure S2. XRD patterns of the prepared SMZ/TMP salt and the SMZ/TMP salt obtained from the Cambridge Structural Database (Refcode: SMZTMP01).

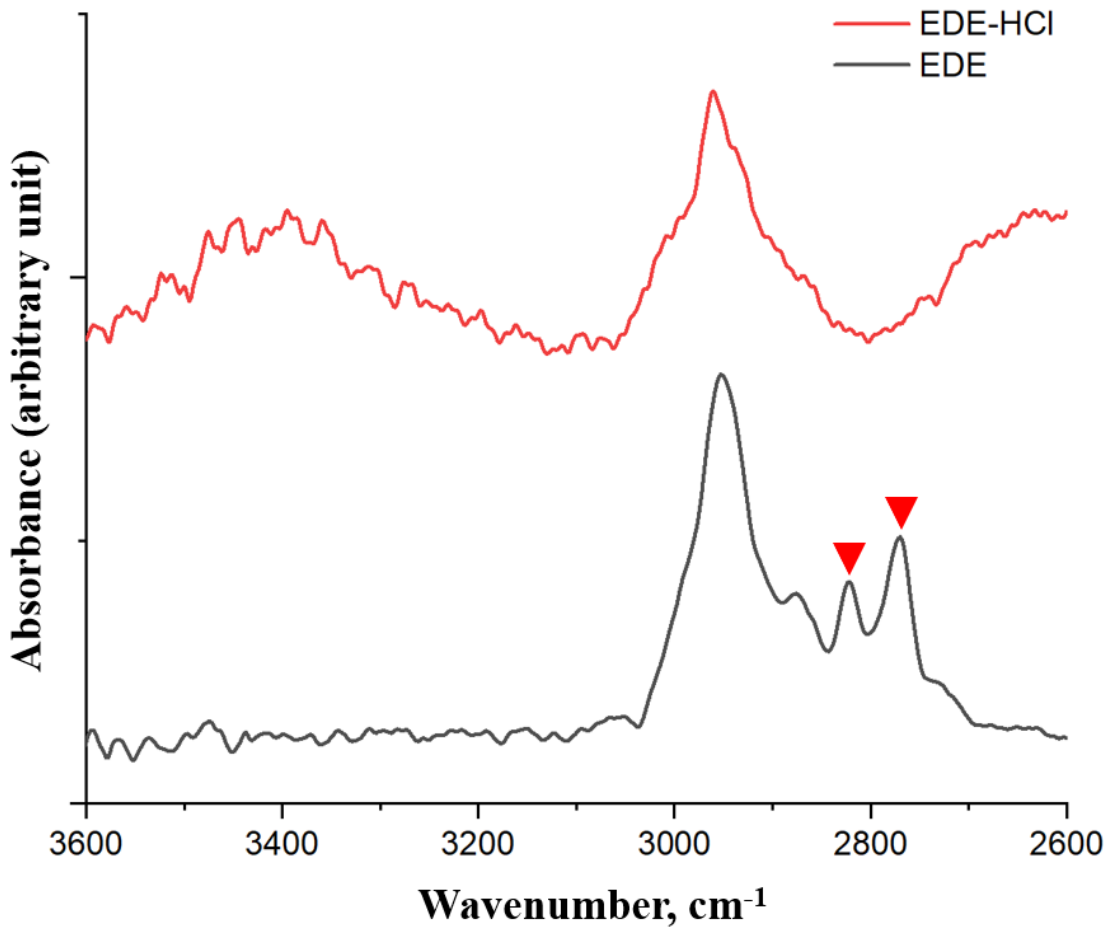

Figure S3. IR spectra of “as is” EDE and EDE-HCl polymer salt (EDE-HCl).

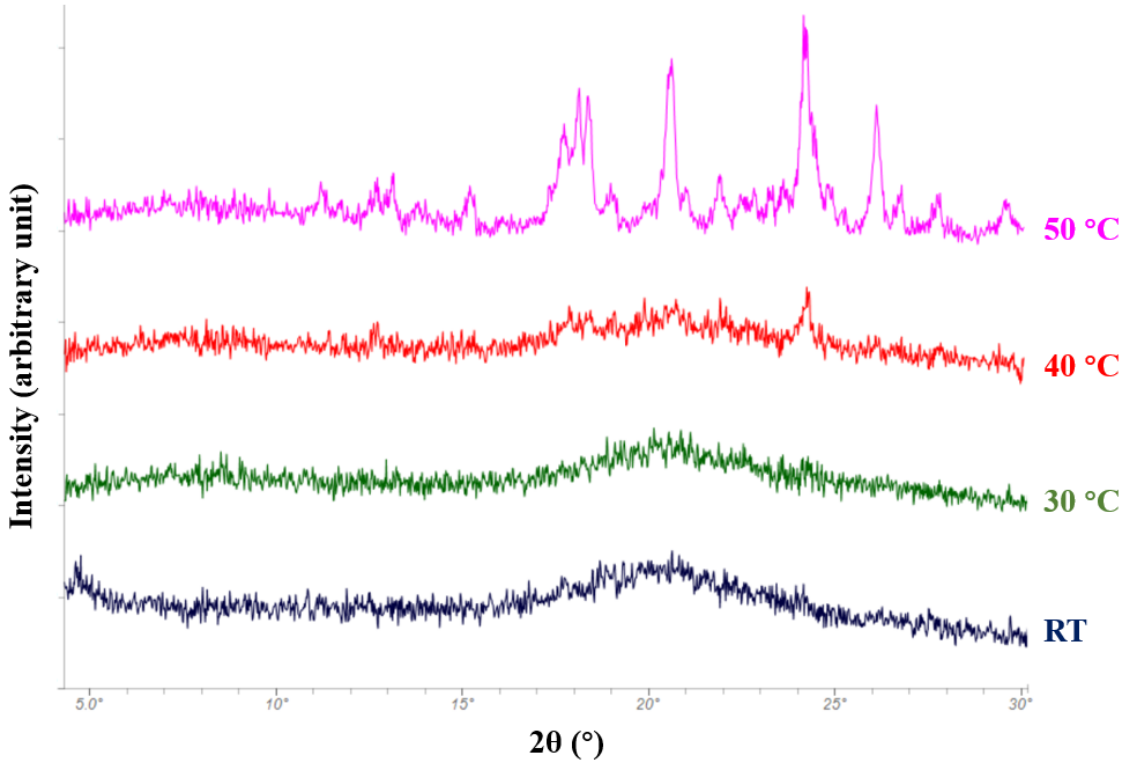

Figure S4. Variable temperature XRD results of amorphous SMZ.

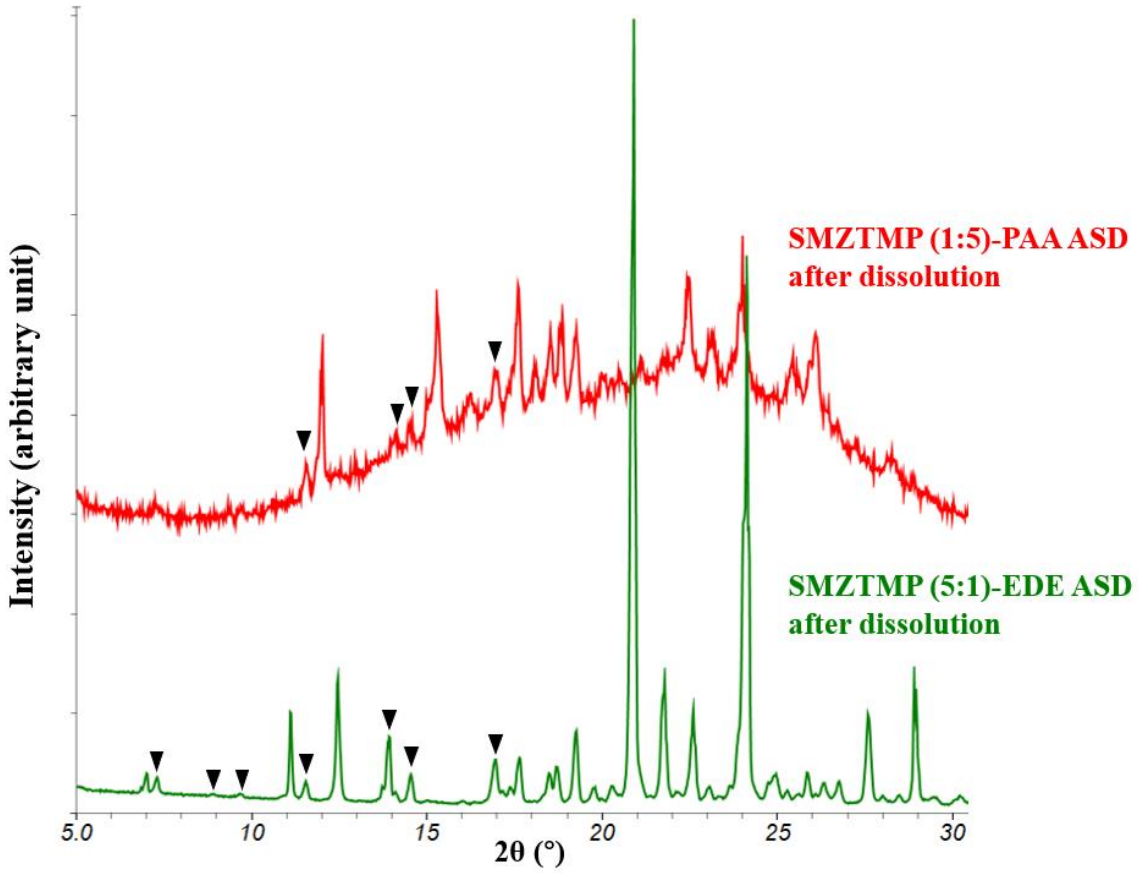

Figure S5. XRD patterns of ternary PAA and EDE ASDs after dissolution. The diffraction peaks of the SMZ/TMP salt are highlighted with black revert triangles.

REFERENCES

1. Kalepu, S.; Nekkanti, V., Insoluble drug delivery strategies: review of recent advances and business prospects. *Acta Pharmaceutica Sinica B* **2015,** *5* (5), 442-453.

2. Newman, A.; Zografi, G., What We Need to Know about Solid-State Isothermal Crystallization of Organic Molecules from the Amorphous State below the Glass Transition Temperature. *Molecular pharmaceutics* **2020,** *17* (6), 1761-1777.

3. Baghel, S.; Cathcart, H.; O'Reilly, N. J., Polymeric amorphous solid dispersions: a review of amorphization, crystallization, stabilization, solid-state characterization, and aqueous solubilization of biopharmaceutical classification system class II drugs. *Journal of pharmaceutical sciences* **2016,** *105* (9), 2527-2544.

4. Hancock, B. C.; Zografi, G., Characteristics and significance of the amorphous state in pharmaceutical systems. *Journal of pharmaceutical sciences* **1997,** *86* (1), 1-12.

5. Han, J.; Wei, Y.; Lu, Y.; Wang, R.; Zhang, J.; Gao, Y.; Qian, S., Co-amorphous systems for the delivery of poorly water-soluble drugs: Recent advances and an update. *Expert opinion on drug delivery* **2020,** *17* (10), 1411-1435.

6. Mistry, P.; Mohapatra, S.; Gopinath, T.; Vogt, F. G.; Suryanarayanan, R., Role of the strength of drug–polymer interactions on the molecular mobility and crystallization inhibition in ketoconazole solid dispersions. *Molecular pharmaceutics* **2015,** *12* (9), 3339-3350.

7. Bhujbal, S. V.; Mitra, B.; Jain, U.; Gong, Y.; Agrawal, A.; Karki, S.; Taylor, L.; Kumar, S.; Zhou, Q., Pharmaceutical amorphous solid dispersion: A review of manufacturing strategies. *Acta Pharmaceutica Sinica B* **2021**.

8. Dengale, S. J.; Grohganz, H.; Rades, T.; Löbmann, K., Recent advances in co-amorphous drug formulations. *Advanced drug delivery reviews* **2016,** *100*, 116-25.

9. Bhardwaj, S. P.; Arora, K. K.; Kwong, E.; Templeton, A.; Clas, S.-D.; Suryanarayanan, R., Correlation between molecular mobility and physical stability of amorphous itraconazole. *Molecular pharmaceutics* **2013,** *10* (2), 694-700.

10. Kothari, K.; Ragoonanan, V.; Suryanarayanan, R., Influence of Molecular Mobility on the Physical Stability of Amorphous Pharmaceuticals in the Supercooled and Glassy States. *Molecular pharmaceutics* **2014,** *11* (9), 3048-3055.

11. Kothari, K.; Ragoonanan, V.; Suryanarayanan, R., The role of drug–polymer hydrogen bonding interactions on the molecular mobility and physical stability of nifedipine solid dispersions. *Molecular pharmaceutics* **2015,** *12* (1), 162-170.

12. Amponsah-Efah, K. K.; Mistry, P.; Eisenhart, R.; Suryanarayanan, R., The Influence of the Strength of Drug–Polymer Interactions on the Dissolution of Amorphous Solid Dispersions. *Molecular pharmaceutics* **2020,** *18* (1), 174-186.

13. Kim, D.-W.; Weon, K. Y., Pharmaceutical application and development of fixed-dose combination: dosage form review. *Journal of Pharmaceutical Investigation* **2021,** *51* (5), 555-570.

14. Jiang, Q.; Hirsh, D. A.; Tu, Y.; Luo, L., Multicomponent crystals of an artemisinin derivative and cinchona alkaloids for use as antimalarial drugs. *CrystEngComm* **2021,** *23* (39), 6843-6847.

15. Caira, M. R., Sulfa drugs as model cocrystal formers. *Molecular pharmaceutics* **2007,** *4* (3), 310-316.

16. Beyer, A.; Grohganz, H.; Löbmann, K.; Rades, T.; Leopold, C. S., Influence of the cooling rate and the blend ratio on the physical stability of co-amorphous naproxen/indomethacin. *European Journal of Pharmaceutics and Biopharmaceutics* **2016,** *109*, 140-148.

17. Qiang, Z.; Adams, C., Potentiometric determination of acid dissociation constants (pKa) for human and veterinary antibiotics. *Water research* **2004,** *38* (12), 2874-2890.

18. Fruttero, R.; Hawkes, G. E.; Randall, E. W.; Gasco, A.; Groombridge, C. J., 13 C and 15 N solution and solid-state nuclear magnetic resonance study of the intermolecular interactions in the 1: 1 trimethoprim sulphamethoxazole complex. *Journal of the Chemical Society, Perkin Transactions 2* **1988,** (10), 1863-1866.

19. Barbosa, J. A.; Abdelsadig, M. S.; Conway, B. R.; Merchant, H. A., Using zeta potential to study the ionisation behaviour of polymers employed in modified-release dosage forms and estimating their pKa. *International journal of pharmaceutics: X* **2019,** *1*, 100024.

20. Duggirala, N. K.; Li, J.; Kumar, N. K.; Gopinath, T.; Suryanarayanan, R., A supramolecular synthon approach to design amorphous solid dispersions with exceptional physical stability. *Chemical Communications* **2019,** *55* (39), 5551-5554.

21. Richert, R.; Stickel, F.; Fee, R.; Maroncelli, M., Solvation dynamics and the dielectric response in a glass-forming solvent: from picoseconds to seconds. *Chemical physics letters* **1994,** *229* (3), 302-308.

22. de Moura Oliveira, C. H.; Freitas, J. T. J.; Rosa, I. M.; Doriguetto, A. C., Thermodynamic Relationship and Phase Transition Study Involving Two Polymorphs of Sulfamethoxazole: Form I vs. Form II. *New Journal of Chemistry* **2021**.

23. Djellouli, F.; Dahmani, A.; Hassani, A., Characterization of the polymorph changes in Trimethoprim. *Journal of Thermal Analysis and Calorimetry* **2017,** *130* (3), 1585-1591.

24. Kwei, T., The effect of hydrogen bonding on the glass transition temperatures of polymer mixtures. *Journal of Polymer Science: Polymer Letters Edition* **1984,** *22* (6), 307-313.

25. Lin, A. A.; Kwei, T.; Reiser, A., On the physical meaning of the Kwei equation for the glass transition temperature of polymer blends. *Macromolecules* **1989,** *22* (10), 4112-4119.

26. Prasad, D.; Chauhan, H.; Atef, E., Amorphous stabilization and dissolution enhancement of amorphous ternary solid dispersions: combination of polymers showing drug–polymer interaction for synergistic effects. *Journal of pharmaceutical sciences* **2014,** *103* (11), 3511-3523.

27. Ueda, H.; Wakabayashi, S.; Kikuchi, J.; Ida, Y.; Kadota, K.; Tozuka, Y., Anomalous role change of tertiary amino and ester groups as hydrogen acceptors in eudragit E based solid dispersion depending on the concentration of naproxen. *Molecular pharmaceutics* **2015,** *12* (4), 1050-1061.

28. Linares, V.; Yarce, C. J.; Echeverri, J. D.; Galeano, E.; Salamanca, C. H., Relationship between degree of polymeric ionisation and hydrolytic degradation of Eudragit® E polymers under extreme acid conditions. *Polymers* **2019,** *11* (6), 1010.

29. Fung, M. H.; Suryanarayanan, R., Effect of organic acids on molecular mobility, physical stability, and dissolution of ternary ketoconazole spray-dried dispersions. *Molecular pharmaceutics* **2018,** *16* (1), 41-48.

30. Wu, W.; Wang, Y.; Löbmann, K.; Grohganz, H.; Rades, T., Transformations between co-amorphous and co-crystal systems and their influence on the formation and physical stability of co-amorphous systems. *Molecular pharmaceutics* **2019,** *16* (3), 1294-1304.

31. Fung, M. H.; DeVault, M.; Kuwata, K. T.; Suryanarayanan, R., Drug-excipient interactions: effect on molecular mobility and physical stability of ketoconazole–organic acid coamorphous systems. *Molecular pharmaceutics* **2018,** *15* (3), 1052-1061.

32. Allesø, M.; Chieng, N.; Rehder, S.; Rantanen, J.; Rades, T.; Aaltonen, J., Enhanced dissolution rate and synchronized release of drugs in binary systems through formulation: Amorphous naproxen–cimetidine mixtures prepared by mechanical activation. *Journal of Controlled Release* **2009,** *136* (1), 45-53.

33. Wang, S.; Heng, W.; Wang, X.; He, X.; Zhang, Z.; Wei, Y.; Zhang, J.; Gao, Y.; Qian, S., Coamorphization combined with complexation enhances dissolution of lurasidone hydrochloride and puerarin with synchronized release. *International journal of pharmaceutics* **2020,** *588*, 119793.

34. Chen, Z.; Zhu, Q.; Qi, J.; Lu, Y.; Wu, W., Sustained and controlled release of herbal medicines: The concept of synchronized release. *International journal of pharmaceutics* **2019,** *560*, 116-125.